ISTANBUL TECHNICAL UNIVERSITY ★ GRADUATE SCHOOL OF SCIENCE ENGINEERING AND TECHNOLOGY

AEROELASTIC ANALYSIS OF 2 DOF TYPICAL AIRFOIL SECTION MODELED WITH SHAPE MEMORY ALLOY SPRINGS

M.Sc. THESIS

Osman DAĞLI

Department of Defence Technologies

Defence Technologies Program

JULY 2020

ISTANBUL TECHNICAL UNIVERSITY ★ GRADUATE SCHOOL OF SCIENCE ENGINEERING AND TECHNOLOGY

AEROELASTIC ANALYSIS OF 2 DOF TYPICAL AIRFOIL SECTION MODELED WITH SHAPE MEMORY ALLOY SPRINGS

M.Sc. THESIS

Osman DAĞLI
(514171019)

Department of Defence Technologies

Defence Technologies Program

Thesis Advisor: Prof. Dr. Metin Orhan KAYA

JULY 2020

İSTANBUL TEKNİK ÜNİVERSİTESİ ★ FEN BİLİMLERİ ENSTİTÜSÜ

ŞEKİL HAFIZALI ALAŞIM YAYI İLE ÖRNEKLENMİŞ İKİ SERBESTLİK DERECELİ KANAT PROFİLİNİN AEROELASTİK ÇÖZÜMLEMESİ

YÜKSEK LİSANS TEZİ

Osman DAĞLI
(514171019)

Savunma Teknolojileri Anabilim Dalı

Savunma Teknolojileri Programı

Tez Danışmanı: Prof. Dr. Metin Orhan KAYA

TEMMUZ 2020

Osman DAĞLI, a M.Sc. student of ITU Graduate School of Science Engineering and Technology 514171019, successfully defended the thesis entitled "AEROELASTIC ANALYSIS OF 2 DOF TYPICAL AIRFOIL SECTION MODELED WITH SHAPE MEMORY ALLOY SPRINGS", which he prepared after fulfilling the requirements specified in the associated legislations, before the jury whose signatures are below.

Thesis Advisor :	**Prof. Dr. Metin Orhan KAYA** Istanbul Technical University	.....
Jury Members :	**Asst. Prof. Dr. Özge ÖZDEMİR** Istanbul Technical University	.....
	Asst. Prof. Dr. Serhat YILMAZ National Defence University	.....

Date of Submission : 15 June 2020
Date of Defense : 16 July 2020

To my family and ÇAPAR family,

FOREWORD

First of all, I would like to thank to my advisor Prof. Dr. Metin Orhan KAYA for his patience, guidance, support, encouragement, and also his extensive knowledge that he shared with me throughout my thesis work. His help had a very beneficial effect.

I would like to thank to the all professors of Faculty of Aeronautics and Astronautics at the Istanbul Technical University. Especially, our coordinator Prof. Dr. Melike NİKBAY for supervising the students of Department of Defence Technologies. Besides, I would like to thank to Asst. Prof. Dr. Vagner Candido de SOUSA from Sao Paulo State University for his assistance.

I would like to thank to my schoolfellows Mahdi MALEKİ and Bilgehan ŞEREF for standing shoulder to shoulder with me since we start to graduate education and their valuable assistance.

I would like to thank to my colleagues from Turkish Air Force Academy Res. Asst. Ukte ÖNER, Asst. Prof. Dr. Serhat YILMAZ, Res. Asst. Berk AĞIN, Mert SEVER, Orhan KARA and Asst. Dr. Col. Mehmet KURUŞCU and all other workmates (UYSAL, AKSEN, TELLİ, ŞEN, GEÇGEL) for their assistance while working on this thesis.

I would like to many thank to the my mother Esma DAĞLI, my father Mustafa DAĞLI, my siblings Merve DAĞLI and Onur DAĞLI whose have been standing by me with their moral and material support during all my life. I would also like to many thank to my almost a quarter centenarian friends Burakcan DEMİRCİ and Ali ÖZGÜL for sharing my highs and lows.

June 2020 Osman DAĞLI

TABLE OF CONTENTS

Page

ABBREVIATIONS

A	: Austenite
A $\rightarrow$ **M**	: Phase Transformation From Austenite to Martensite
A $\rightarrow$ $\mathbf{M^d}$	: Phase Transformation from Austenite to Detwinned Martensite
A $\rightarrow$ $\mathbf{M^t}$	: Phase Transformation from Austenite to Twinned Martensite
CG	: Center of Gravity
EA	: Elastic Axis
LCO	: Limit Cycle Oscillation
M	: Martensite
$\mathbf{M^d}$	: Detwinned Martensite
$\mathbf{M^t}$	: Twinned Martensite
M $\rightarrow$ **A**	: Phase Transformation From Martensite to Austenite
$\mathbf{M^d}$ $\rightarrow$ **A**	: Phase Transformation from Detwinned Martensite to Austenite
$\mathbf{M^t}$ $\rightarrow$ **A**	: Phase Transformation from Twinned Martensite to Austenite
$\mathbf{M^t}$ $\rightarrow$ $\mathbf{M^d}$	: Phase Transformation from Twinned Martensite to Detwinned Martensite
SÇS	: Sınır Çevrimli Salınım
SMA	: Shape Memory Alloy
SME	: Shape Memory Effect
ŞHA	: Şekil Hafızalı Alaşım
ŞHE	: Şekil Hafızası Etkisi

SYMBOLS

h	: Plunge displacement
α	: Pitch displacement
U	: Airflow speed
a	: Non-dimensional distance between the half chord and EA
b	: Half chord length
x_α	: Non-dimensional distance between the EA and CG
l	: Span length
k_h	: Plunge stiffness per unit span length
k_α	: Pitch stiffness per unit span length
d_h	: Plunge damping coefficient
d_α	: Pitch damping coefficient
δ	: Variation
T_E	: Total kinetic energy
V_E	: Total potential energy
W_{nca}	: Virtual work of aerodynamic loadings
W_{sd}	: Virtual work of aerodynamic dampings
m	: Airfoil mass per unit span length
m_f	: Effective fixture mass per unit span length
I_α	: Inertial moment
q_i	: Generalized coordinate
Q_i	: Non-conservative force
r_α	: Gyration radius
$\tilde{h}$	: Dimensionless plunge displacement
ω_h	: Plunge natural frequency
ω_α	: Pitch natural frequency
μ	: Mass ratio
t	: Dimensional time

$\tilde{t}$: Dimensionless time

ζ_h : Plunge damping ratio

ζ_α : Pitch damping ratio

η_α : Natural frequency ratio

M_α : Aerodynamic pitch moment

L : Aerodynamic lift force

$\tilde{M}_\alpha$: Dimensionless aerodynamic pitch moment

$\tilde{L}$: Dimensionless aerodynamic lift force

$\mathbf{I}$: Identity matrix

$\mathbf{M_s}$: Dimensionless mass matrix

$\mathbf{K_s}$: Dimensionless stiffness matrix

$\mathbf{B_s}$: Dimensionless damping matrix

ρ : Pitch displacement

$C(\kappa)$: Theodorsen function

ρ : Reduced frequency

x_{a_i} : Augmented aerodynamic states

$\mathbf{x_a}$: Aerodynamic state vector

$\mathbf{S_i}$: Circulatory aerodynamic vectors

$\mathbf{D}$: Aerodynamic coupling in the structural equations

$\tilde{D}$: Non-dimensional D matrix

$\mathbf{R}$: Circulatory aerodynamic vector

$\mathbf{M}$: Total mass matrix

$\mathbf{K}$: Total stiffness matrix

$\mathbf{B}$: Total damping matrix

$\mathbf{M_{nc}}$: Non-circulatory addition to mass matrix

$\mathbf{K_{nc}}$: Non-circulatory addition to stiffness matrix

$\mathbf{B_{nc}}$: Non-circulatory addition to damping matrix

$\mathbf{E_i}$: Aerodynamic to structural coupling terms

$\tilde{E}_i$: Non-dimensional aerodynamic to structural coupling terms

$\mathbf{F_p}$: Aerodynamic terms

$\tilde{F}_p$: Non-dimensional aerodynamic terms

$\mathbf{A}$: Dimensionless aeroelastic matrix

$\mathbf{x}$: Dimensionless aeroelastic state vector

M_s : Martensitic phase start temperature

M_f : Martensitic phase finish temperature

A_s : Austenitic phase start temperature

A_f : Austenitic phase finish temperature

τ_s^{min} : Minimum martensitic phase start shear stress

τ_f^{min} : Minimum martensitic phase finish shear stress

τ_s^M : Martensitic phase start shear stress

τ_f^M : Martensitic phase finish shear stress

τ_s^A : Austenitic phase start shear stress

τ_f^M : Austenitic phase finish shear stress

τ : Shear stress

σ_s^{min} : Minimum martensitic phase start stress

σ_f^{min} : Minimum martensitic phase finish stress

σ_s^M : Martensitic phase start stress

σ_f^M : Martensitic phase finish stress

σ_s^A : Austenitic phase start stress

σ_f^M : Austenitic phase finish stress

σ : Stress

E : Elastic modulus

E_M : Martensitic elastic modulus

E_A : Austenitic elastic modulus

G : Shear modulus

γ : Shear strain

ε : Strain

ε_{res} : Residual strain

Ω : Transformation factor

Θ : Thermal expansion coefficient

T : Temperature

μ_p : Poisson's ratio

ξ : Martensite fraction

ξ_t : Twinned martensite fraction

ξ_d : De-twinned martensite fraction

G_M : Martensitic shear modulus

G_A : Austenitic shear modulus

F : External force

f_i^{sma} : SMA spring force

R : Spring coil radius

r : Spring wire radius

N : Number of active coils

LIST OF TABLES

Page

LIST OF FIGURES

Page

AEROELASTIC ANALYSIS OF 2 DOF TYPICAL AIRFOIL SECTION MODELED WITH SHAPE MEMORY ALLOY SPRINGS

SUMMARY

In the area of aeroelasticity, the most dangerous physical phenomena is flutter which is dynamic instability where aerodynamic, structural and inertial forces interacts and leads to oscillate an airfoil increasingly out of control. This phenomena causes destructive structural failures and violent damages to aircrafts. Shape memory alloys (SMA) are specific materials owning speciality of recovering strains up to useful level. Basically, SMAs can restore deformed shape, caused by some loadings, to its original condition. This speaciality provides energy dissipation and passive vibration control.

The fundamental idea of this thesis is to present the modelling, numerical analysing, comparing, verifying and observing the effects of two degrees of freedom two-dimensional aeroelastic airfoil section by changing the linear steel spring with SMA spring. The actual aim is to examine the influences of superelastic hysteresis of the SMA on the aeroelastic behaviors of a aircraft wing section. The SMAs show special nonlinear properties in contrast to the other materials which are often called the superelasticity and shape memory effect (SME). This property occurs as a result of phase transformation under particular thermal and mechanical loadings to the SMA and this transformation process identified with a validated and applicable model.

In the area of aeroelasticity, the most dangerous physical phenomenon, flutter, is a dynamic instability in which aerodynamic, structural and inertial forces interact and increasingly cause a wing structure to get out of control. This phenomenon causes destructive structural failures and severe damage to aircraft. SMAs are special materials with the ability of recovery of shape changes to a beneficial level. Basically, SMAs can restore its deformed shape caused by some loads to its original shape. This property provides energy dissipation and passive vibration control. In this context, superelastic properties of shape memory alloys can be used to dampen dangerous level oscillations that may occur in the wings. By absorbing the high level of energy that oscillations can create, flutter formation can be delayed somewhat or converted to limit cycle oscillations (LCO).

The influences of introducing the SMA spring into the equation of motion of linear two degrees of freedom two-dimensional aeroelastic airfoil section are investigated. Also, with the purpose of state the aerodynamic loads, unsteady aerodynamic model was used. The complete model was written in the state-space form to get the solutions of the equation of motion with the classical integration schemes and fourth order Runge Kutta method was selected to solve the complete model.

First of all, Ni-Ti alloy which is also called Nitinol was selected as a SMA material to use in this work due to its best response, excellent structural and workability properties. Besides that, modelled as a helical springs for replacing with linear steel

spring in aeroelastic typical section. Then, the equations are solved for both springs and responses of linear steel spring and SMA spring was compared.

Secondly, the external loads was applied to the SMA spring to indicate their natural damping properties. Later, results of flutter and post-flutter behaviors of the aeroelastic system where Ni-Ti SMA spring shows its nonlinear influences analyzed. Then, the outputs are compared whether they match with previous works.

It has been numerically seen when examined the results of the solutions, the SMA springs' superelastic hysteresis was utilized efficiently to suppress the unstable growing oscillations and generate the acceptable LCOs on some different airflow speeds.

ŞEKİL HAFIZALI ALAŞIM YAYI İLE ÖRNEKLENMİŞ İKİ SERBESTLİK DERECELİ KANAT PROFİLİNİN AEROELASTİK ÇÖZÜMLEMESİ

ÖZET

Son yıllarda, havacılık, savunma ve ileri imalat sanayileri için yüksek performanslı yapısal ve mekanik sistemlere olan güçlü talep, ileri malzemelerin gelişimini teşvik etmiştir. Genel olarak, klasik malzemeler, çevre ortamdaki değişikliklere cevap veremedikleri ve edimsel olarak tasarlanmadıkları hizmet koşullarında çalışamayacakları anlamında pasiftir. Bu nedenle, değişken çalışma koşulları tüm pratik uygulamalarda ortaya çıkabileceğinden, elastodinamik tepkisi geniş bir hizmet yelpazesi altında gerçek zamanlı olarak en uygun şekilde uyarlanabilen ileri aktif malzemelerin gelişimine önemli bir ihtiyaç vardır. Örneğin, akıllı malzemeler ve yapılar hem piezoelektrik malzemeler ve şekil hafızalı alaşımlar (ŞHA) tarafından sunulan güçlü özelliklerden hem de algılama özelliklerinden faydalanır.

Şekil hafızalı alaşımlar, başlangıçta uygun termomekanik koşullar altında şekli bozulursa veya şekillendirilirlerse, daha yüksek bir sıcaklığa ısıtıldıktan sonra başlangıç şekilleri geri kazanılabilir. Alaşım malzemesi özelliklerine ve dış koşullara bağlı olarak, şekil geri kazanımı iki şekilde gerçekleşebilir:
- Malzeme düşük sıcaklıkta şekli bozulursa, ayırt edici bir sıcaklığın üzerine ısıtılarak başlangıç şekli geri kazanılabilir. Bu özellik şekil hafızası etkisi (ŞHE) olarak bilinir;
- Malzeme yüksek sıcaklıkta şekli bozulursa, uygulanan yük kaldırılarak başlangıç şekli geri kazanılabilir. Bu özellik süperelastisite olarak bilinir.

Şekil hafızalı alaşımlar ayrıca martensitik durumda ve iki fazlı durumda yüksek bir sönümleme yetisine sahiptir. Mekanik enerjinin ısıya dönüşümünü içeren sönümleme yetisi, sadece şekil hafızalı alaşımlara özgü ayırt edici bir davranış değildir. Tüm malzemeler bu özelliği sergiler. Fakat, ŞHAlar standart malzemelerinkinden daha büyük bir sönümleme yetisi sergilerler. Süperelastik yükleme ve boşaltma arasındaki gerilim histerezisinin bir sonucu olarak fazla enerji sönümlenir.

Aeroelastisite; bir çalışma konusu olarak, aerodinamik kuvvetler ile elastik bir yapının tepki kuvvetleri arasındaki etkileşimleri açıklar. Aerodinamik kuvvetler elastik bir yapının şeklini bozar ve yapının şekil değişimi, üzerine etkiyen aerodinamik kuvvetlerin doğasını değiştirir. Dinamik bir sistemde, bu kuvvetler birbirlerini geri besleyebilir ve bazen karmaşık ve tahmin edilmesi zor tepkilere neden olabilir. Belirli koşullar altında, dinamik sistemin geri besleme yapısı, çırpınma (flutter) gibi yapıda fiziksel hasara sebep olan kararsızlıklara yol açabilir.

Aeroelastisite alanında, en tehlikeli fiziksel olgu olan çırpınma, aerodinamik, yapısal ve atalet kuvvetlerinin etkileşime girdiği ve gittikçe artarak bir kanat yapısının kontrolden çıkmasına neden olan dinamik bir kararsızlıkdır. Bu olgu, yıkıcı yapısal arızalara ve uçaklarda şiddetli hasarlara neden olur. ŞHAlar, şekil değişimlerinin

faydalı seviyeye kadar geri kazanımına sahip özel malzemelerdir. Temel olarak, ŞHAlar, bazı yüklemelerden kaynaklanan bozulmuş şeklini başlangıç durumuna geri getirebilir. Bu özellik, enerji dağılımı ve pasif titreşim kontrolü sağlar. Bu bağlamda, kanatlarda oluşabilecek tehlikeli seviyedeki salınımların sönümlendirilmesinde şekil hafızalı alaşımların süperelastik özelliklerinden faydalanılabilir. Salınımların yaratabileceği yüksek seviyedeki enerji soğurularak çırpınma oluşumu bir miktar geciktirilebilir veya sınır çevrimli salınımlara (SÇS) dönüştürülebilir.

Bu tezin temel fikri iki serbestlik dereceli iki boyutlu aeroelastik tipik kanat kesitinin yunuslama ve dalma yaylarıyla örneklenmesi, sayısal çözümlemesi, yazınla karşılaştırılması ve doğrulanmasıdır. Asıl amaç ise, şekil hafızalı alaşımın süperelastik histerezisinin bir uçak kanadı kesitinin aeroelastik davranışları üzerindeki etkilerini incelemektir. ŞHAlar, genellikle ŞHE ve süperelastisite olarak adlandırılan, diğer malzemelerin aksine özel doğrusal olmayan bir özellik gösterir. Bu özellik, şekil hafızalı alaşıma özel ısıl ve mekanik yükler altında, martezit fazdan östenit faza veya östenit fazdan martenzit faza doğru olan faz dönüşümünün bir sonucu olarak ortaya çıkar ve bu dönüşüm işlemi, doğrulanmış ve uygulanabilir bir örnekle tanımlanır. Bu bağlamda, ŞHAlar için kayma gerilimi ve kayma şekil değişimini içeren bir boyutlu Liang-Rogers örneği kullanılmıştır.

İlk olarak, Nitinol olarak da adlandırılan Ni-Ti alaşımı, en iyi tepki, mükemmel yapısal ve işlenebilirlik özellikleri nedeniyle bu çalışmada kullanılmak üzere ŞHA malzemesi olarak seçilmiştir. Bununla birlikte, aeroelastik tipik kanat kesitindeki doğrusal yaylarla değiştirmek için Nitinol ŞHA malzemesi helisel yay olarak örneklenmiştir. ŞHA yayının, doğrusal iki serbestlik dereceli iki boyutlu aeroelastik tipik kanat kesitinin hareket denklemine dahil edilmesinin etkileri araştırılmıştır. Araştırmamızda dalma yer değiştirmesinin, yunuslama yer değiştirmesine göre etkileri küçük olup gözlemlemesi zor olacağından dolayı sadece yunuslama yayı ŞHA yayıyla değiştirilmiştir. Ayrıca, aerodinamik yükleri belirtmek amacıyla, düzensiz aerodinamik örnek kullanılmıştır. Daha sonra, elde edilen hareket denklemleri sistemi, klasik integrasyon şemaları ile çözmek ve sonuçları elde etmek için durum-uzay formunda yazılmıştır. Tüm sistemi çözmek için klasik integrasyon yöntemlerinden biri olan dördüncü dereceden Runge-Kutta yöntemi seçilmiştir.

İkinci aşamada, hareket denklemi sistemleri doğrusal çelik yaylar baz alınarak çözülmüş ve sistemin doğal davranışları, doğal frekansları ve özdeğer çözümlemesi yapılarak doğrusal çırpınma hızı belirlenmiştir. Daha sonra denklemler sistemi, her iki yay için çözülmüş, doğrusal çelik yay ve ŞHA yayının cevapları karşılaştırılmıştır.

Üçüncü aşamada, doğal süperelastik yani sönümleyici ve dağıtıcı özelliklerini göstermesi için gerekli olan koşullar şekil hafızalı alaşıma uygulanmıştır. Bunlar östenit faz geçişinin bittiği sabit sıcaklık ve doğrusal olmayan özelliğinin açığa çıkması için gereken kritik kayma gerilmesi büyüklüğüdür. Bu kayma gerilmesi büyüklüğüne ulaşabilmek için yunuslama yaylarına harici ön yüklemeler uygulanmıştır. Daha sonra, Ni-Ti ŞHA yayının aeroelastik sistemin çırpınma ve çırpınma sonrası davranışlarının sonuçları çözümlenmiştir. Ardından elde edilen cevapların, önceki çalışmalarla eşleşip eşleşmedikleri karşılaştırılmıştır.

Çözümlerin sonuçları incelendiğinde, ŞHA yaylarının kritik kayma gerilmesine ulaşılmadığında doğrusal çelik yay gibi davrandığı ve sönümleyici ve dağıtıcı özelliklerini açığa çıkarmadığı gözlemlenmiştir. ŞHA yaylarının süperelastik histerezisinden, kararsız büyüyen salınımları bastırmak ve bazı farklı hava akış

hızlarında kabul edilebilir sınır döngü salınımları (LCO) oluşturmak için verimli bir şekilde faydalanıldığı görülmüştür.

1. INTRODUCTION

In these days, the defense, aerospace and manufacturing industries that require smart and high-quality structural systems have led to the development of advanced materials. Simply, materials that interact with its environment and can respond to environmental influences are defined as smart materials. Classical materials are considered as passive because they cannot respond to changes in the environment and smart materials are considered as active. For example, smart materials and structures are those that take advantage of the powerful features offered by morphing structures, piezoelectric materials and shape memory materials as well as sensing properties. Therefore, unlike classical materials, smart materials are sensitive to stimuli and have strong abilities to compensate for undesired effects. The most popular engineering case that uses smart materials is vibration control and damping. There are two approaches in control of vibration with using smart materials as active and passive. In active control, smart materials are used as an actuator. In passive control, reducing vibrations with energy dissipating to limited magnitudes is seen. Shape memory alloys can be used both active and passive control approaches. In active applications, SMAs are used as thermomechanical actuators. Due to the superelastic effect of SMAs, the hysteretic behavior employs vibration damping properties.

Aircraft aeroelasticity problem as always continued that importance while the first aircraft has introduced even with complexity of modern aircraft the importance of this problem has intensified. One of the most common aeroelasticity problem capable of catastrophic destruction which encountered in aircrafts is flutter instability.

1.1 Purpose of Thesis

The aim of this thesis is to model the classical aeroelastic airfoil section with SMA springs, to perform numerical analysis, and to examine the effects on flutter and post-flutter speeds. Studies on aeroelasticity, vibration control and smart materials were examined. In these studies, it has been observed that generally piezoelectric

materials and SMAs are used. However, there are not many studies on the use of SMAs in aeroelastic analysis. For this reason, in this thesis, it is aimed to model the classical aeroelastic airfoil section with SMA springs, to investigate and analyze their behavior under different load and velocity conditions. To alter the flutter behavior of the aeroelastic airfoil section, it can be utilized from the capacity of the adjustable elastic properties of SMAs. In this thesis, it focuses on the use of superelastic hysteresis of SMA springs as a completely passive damping mechanism to change the aeroelastic behavior of the typical section.

1.2 Literature Review

The influences and applications of the nonlinear hysteretic behavior and damping effects of SMAs due to the phase transformations caused by temperature or stress have been examined in the literature. In Gandhi and Chapuis' study, an unclamped vibrating beam and symmetrically mounted pseudoelastic SMA wires are taken into account to obtain the essentials of the SMA damping configuration and system parameters as well as the effects of excitation loads on the performance of the SMA based structural damping behavior [1].

Machado and Lagoudas are presented an investigation of a one degree of freedom SMA oscillator which includes preloaded SMA wires on a SMA damping device. The good harmony is seen in experimental and numarical results [2].

In Fosdick and Ketema's work, the usability and general macroscopic characteristics of a SMA wire as a passive vibration damper in a dynamic system is examined [3]. Attention focuses on passive control devices which introduces spcial base isolator bars with SMA material. They say, laboratory tests highlight how material properties and thermal processes can lead to undesirable properties, as the viscous behavior detected for the current Ni - Ti alloy is under constant load. Its existence will cancel out most of the benefits of adopting SMA and should therefore be carefully avoided [4].

Biffi et al. are investigated a composite that is containing material made of fiberglass laminated matrix and embedded SMA layers in the material. As a result, it was found that displacement decreased exponentially and the amplitude reduction rate was proportional to the damping properties of the beam [5]. In the study of Aguiar et al.,

SMA helical springs are considered and modeled as a classic approach for linear elastic springs. The thermomechanical behavior of the SMA helical springs was examined by experimental tests with different thermomechanical loads [6].

Also, the constitutive models which is explained variously (one dimensional, two dimensional and other complex models) can be found in the literature. Tanaka et al. presented a one-dimensional model considering the exponential hardening laws for the martensite fraction, which represents the internal variable of the material during phase transitions, and assuming that the material properties are constant during phase transitions. In Tanaka's study, the pseudoelastic effect and shape memory effect resulting from phase transformations of some alloy materials were investigated thermomechanically. Thermomechanical constitutive equations and transformation kinetics are applied to explain the stress, strain and temperature behavior of the alloys. In contrast to Tanaka et al.'s work, Liang and Rogers proposed a cosine-based function to refer the martensite fraction evolution as a internal variable. Liang and Rogers presented a one-dimensional structural model related to shape memory materials. The thermomechanical model here examines the important material properties related to phase transformation of SMAs such as damping behavior, pseudoelasticity and energy distribution in the material managing the SME. In Brinson's study, a one-dimensional model was developed for the thermomechanical behavior of SMAs, based on previous studies of Liang and Tanaka, and in which material functions were not considered constant. The internal variable, called the martensite fraction, is divided into two variables which are temperature-induced and stress-induced. As in Liang and Rogers' work, the evolution of internal variables is governed by a cosine-based function and includes variable elastic stiffness functions during phase transformations [7] [8] [9] [10].

In literature, there are several numerical and experimental applications of SMA material to the helical spring design which is used in this work. Because of the the elasticity modulus of the austenite phase of SMAs is three to four times bigger than martensite phase, it is said that a spring made of SMA can change its spring constant by three to four times. So, this property can provide recovery stress and damping capacity which may be useful in vibration control [11] [6].

There are various static and dynamic problems in aeroelasticity, but the most researched and destructive problem in them is the flutter. According to the literature, the system is stable for airflow speeds smaller than the linear flutter speed and tends to return to the initial conditions. Airflow speeds smaller than linear flutter speed lead to instability and self-sustained increasing vibration amplitudes. There are several types of nonlinearity in aeroelastic systems. These are usually freeplay or bilinear nonlinaerity, geometric or structural nonlinearity and aerodynamic nonlinearities. As a result of such nonlinearities, the vibration amplitudes of the system are converted to limit cycle oscillations below or above the linear flutter speed. Vibrations that exist at a certain bounds are called LCO. These conversion mechanisms are given in Fig. 1.1 with increasing airlow speed. In Fig. 1.1 (a), while the system is stable up to linear flutter speed, LCO increases after linear flutter speed due to some nonlinear effects. The LCO mechanism in Figure 1 (b) causes both stable (straight line) and unstable (dashed line) LCO below the linear flutter speed and this is an undesirable situation [12] [13].

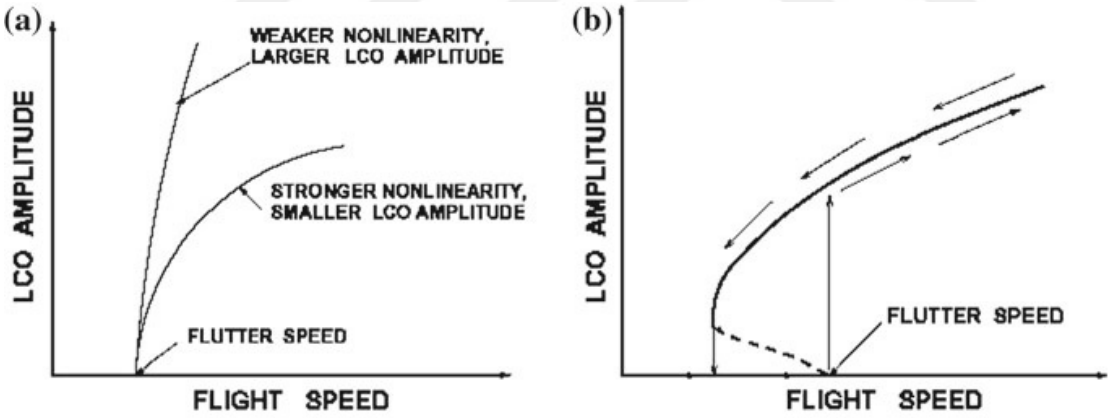

Figure 1.1 : LCO responses with increasing airflow speed (a) Supercritical and (b) Subcritical nonlinearities [13].

Also in literature, the use of SMA materials in aeroelastic systems is investigated. The smart materials have better performance in decreasing the destructive effects of aeroelastic problems than the traditional methods. In Ostachowicz et al.'s work, the effects of a composite plate embedded with SMA fibers on stress-strain relations, vibration modes, natural frequency and thermal buckling are investigated. As a result, the effectiveness of reinforcing composite plates with SMA fibers on vibration control is observed [14]. In Barzegari's article, the effects of SMA wires which is embedded in a cantilever wing on the natural frequency, fluttering and LCO amplitude

are investigated. The effects of pre-strain, temperature and number of SMA wires on aeroelastic properties were taken into consideration. Significant improvements are achieved in aeroelastic behaviors depending on the in-plane load of the SMA wires [15]. Donadon and Faria are investigated the aeroelastic stability and flutter boundary in hybrid composite laminates consisting of SMA wires and continuous carbon fibers embedded in a polymeric matrix material. The study shows that the stiffness caused by changes in the martensite fraction during phase transformation reduces the rate of flutter formation by stabilizing the plate. Thus, the formation of flutter speed can be controlled by controlling the temperature of the SMA wires and the design of the geometric properties [16] The effect of a hysteretic damper on post-critical LCOs is investigated during the formation of airfoil flutter. An aeroelastic model including large amplitude motions and having two degrees of freedom in pitch and plunge motions is considered for plate. SMA spring is then used to control flutter oscillations. The study reveals the ability of SMA springs to reduce the amplitudes of LCOs caused by flutter instability [17]. In this article, Sousa and Marqui are stated that the model of aeroelastic airfoil section with changing the linear steel spring with SMA spring. The state-space representation and Theodorsen aerodynamic approach is used for the simulations. Then, it is analyzed with this modified model at flutter and post-flutter regimes and compared the results with the clasical model. Subsequently, The damping effects of SMA due to the nonlinear hysteretic behavior and LCOs are observed [18].

1.3 Overview

In this section, the subject of the thesis, related field, literature review and the purpose of the thesis are briefly explained. Brief information is given about aeroelasticity, flutter and shape memory alloys. The importance of SMA materials for aeroelastic analysis and their effects on flutter behavior are explained.

Chapter 2 contains basic information on SMA phase transformation behavior with SMA spring modeling. Detailed SMA material properties, phase transformations, damping capabilities and applications, and SMA spring design are described.

Chapter 3 gives an analytical explanation of the typical sectional model. Detailed aeroelastic system, equations of motion and the incorporation of SMA spring into the aeroelastic system are discussed. A state-space model is presented, which includes

equations of motion combined with the SMA springs of the typical section and the unsteady aerodynamic model used to determine aerodynamic loads.

Chapter 4 proposes the general aeroelastic behavior of the typical section with SMA springs at the flutter and post-flutter speeds. The main purpose is concerning the effects of applied preloads to the SMA springs. Specifies the classical aeroelastic airfoil section analysis and structural behavior of SMA springs. Then, investigates the SMA spring (at pitch degrees of freedom) aeroelastic system behavior and some preload values at linear flutter and post-flutter velocities.

Chapter 5 summarizes results of this work. A brief information of the proposed model along with the analysis is presented.

2. SHAPE MEMORY ALLOYS

In this chapter, the basic models, basic ideas and general behaviors of SMAs will be discussed and presented. Following that, the main concept and the model of SMA helical spring which will be used in this thesis will be announced. Later, this helical spring modeled with SMA material will be inserted in the equation of motions of two degrees of freedom of aeroelastic airfoil section to analyse and observe the influences of its superelastic properties.

Basically, the particular property of some materials that have ability of to restore their original shape after deformation caused by some external excitations such as thermal and mechanical loads is called shape memory [19]. Different materials like ceramics, shape memory polymers and shape memory alloys can exhibit shape memory property but, NiTi shape memory alloy which is also called Nitinol is of concern in this thesis because of its sufficient specialities, availability and common usage in literature [20].

2.1 The Perspective of Shape Memory Alloys

If SMAs are initially changed their shapes or deformed under critical thermal and mechanical loads, they can recover their initial form when heated to a higher temperature. Shape recovery and nonlinear properties of SMAs can take place in two ways, depending on the properties of the alloy materials and externally applied loads. The first one is SME which occurs when the shape memory material is deformed at under critical temperature, it can recover its initial shape with heating over critical temperature. The other one is superelasticity which occurs when the shape memory material is deformed at over critical temperature, it can recover its initial shape with unloading the applied mechanical load.

This shape recovery property results from the fact that the crystal structures of the materials are completely recyclable, and most metals and alloys do not. In most crystal structure transformations, even if the material consists of only one atom, atoms move by diffusion. In other words, it changes its composition regionally. However,

materials with shape recovery property move together to create a new structure instead of diffusion. All atoms are pushed to two opposite sides simultaneously and shifted from a square structure to form a new parallelogram structure instead diffusion of atoms.

2.2 Phase Transformations of Shape Memory Alloys

Shape memory alloys have two crystal regions with different crystal structures and properties, namely martensite (M) and austenite (A). As well as the phase emerging at relatively high temperatures is austenite, it has a body-centered cubic crystal structure. Likewise, at relatively low temperatures, the material is in the martensite phase region and can has a tetragonal, orthorhombic or monoclinic crystal structure. The compilation of martensitic variants can take place in two different forms, the twinned martensite (M^t) which is formed by a combination of self-accommodated martensitic variants, and the de-twinned martensite (M^d) which is dominated by a particular variant. Phase transformations from austenite to martensite ($A \rightarrow M$) and from martensite to austenite ($M \rightarrow A$) form the basis for the shape recovery property seen in SMAs [21].

During the cooling process without any applied load, the crystal structure changes from austenite to martensite. This phase transition, resulting in the formation of various martensitic variants, is called forward phase transformation. The arrangement of variants results in twinned martensite and their macroscopic shape changes become negligible. When the material is heated, it returns from the martensitic phase to the austenite phase, without any deformation. This transition is called reverse phase transformation.

These phase transformations reveal a temperature and stress hysteresis. Therefore, temperature-induced or stress-induced transformation must be defined by more than one temperature or stress value. In fact, there are four specific temperatures associated with temperature-induced phase transformation. In the absence of loading on the material, the temperature at which the austenite phase begins to turn into a twinned martensite phase is called the martensite start temperature (M_s), and the temperature at which it converts to fully twinned martensite is called the martensite finish temperature (M_f). As a result, the material is in the fully twinned martensitic phase and the

transformation ends at this point. Likewise, when the material is heated, the same transformation stages begin in the opposite direction at the austenite start temperature (A_s), and the transformation is completed at the austenite finish temperature (A_f). The temperature-induced transformation hysteresis is shown in Figure 2.1.

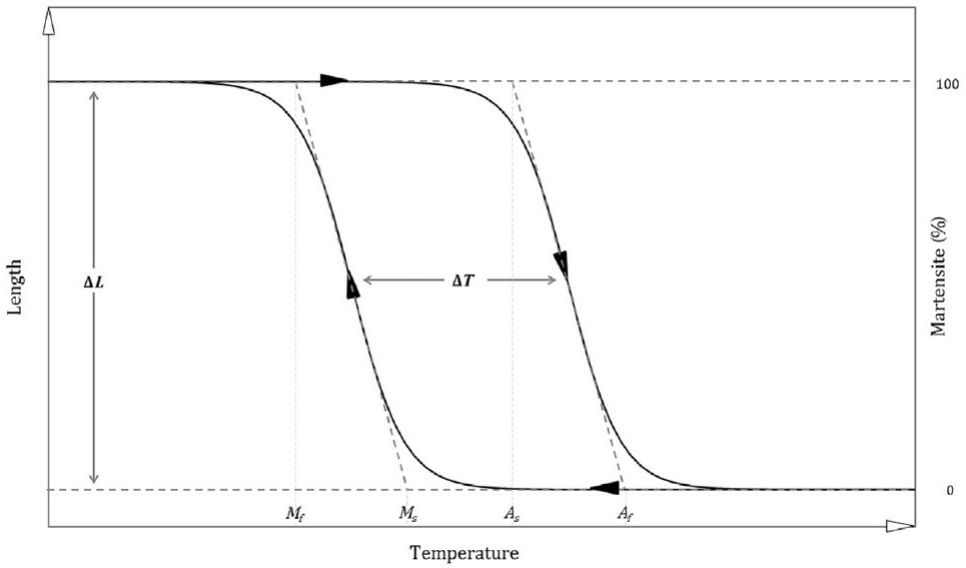

Figure 2.1 : Temperature-Induced Phase Transformation [20].

Also, a diagram for the transformations between SMA crystal structures which are twinned martensite with monoclinic crystal structure and austenite with body-centered cubic crystal structure in Figure 2.2.

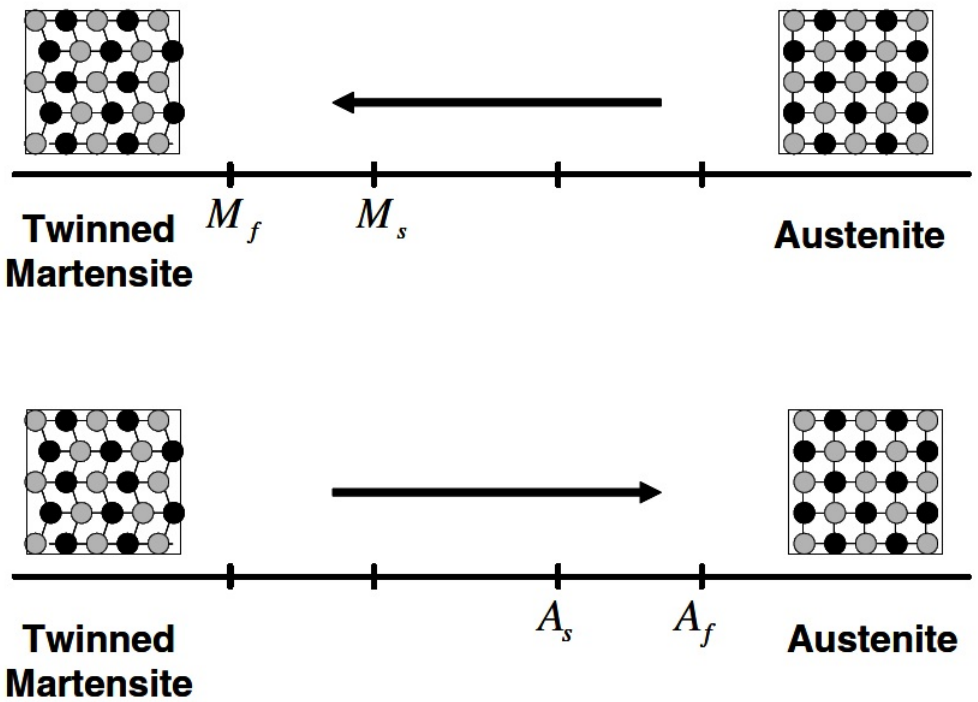

Figure 2.2 : Temperature-Induced Phase Transformation [21].

Specific temperatures for phase transformation increase in direct proportion to the stress applied to SMAs and depending on the material characteristic. The minimum stress values required for the start and finish of a stress-dependent phase transformation are called σ_s^{min} and σ_f^{min}, respectively. Therefore, the stress values required for the start and finish of a stress-dependent phase transformation depending on the temperature values may be higher of the SMAs than the minimum values mentioned above. These new stress values, which change with the temperature of the material, are called σ_s^M and σ_f^M. Likewise, the decreasing stress values required for the recovery of the austenitic phase are called σ_s^A and σ_f^A respectively.

If we assume that a SMA is under the martensite finish temperature without applied load or deformation, this kind of shape memory material is in the twinned martensite phase. A mechanical load to be applied to the SMA becomes possible to converse the twinned martensitic phase to the de-twinned martensitic phase by redirecting a certain number of martensitic variants. When the applied load is removed, the de-twinning process ends with permanent and observable large deformations occurring in the material. After that, the deformed shaped SMA will recover its initial shape if the material is heated above the austenite finish temperature and reverse phase transformation from de-twinned martensite to austenite will be completed. Then, if the SMA material is cooled back under the martensite finish temperature, the twinned martensite phase will gain again with any observable shape deformation.

2.3 Properties and Applications of Shape Memory Alloys

The engineering applications and functional properties of SMAs are related to the phase transitions that occur in its crystal structures. The SME is based on one-way and two-way temperature-induced phase transformation. As for, superelasticity is a result of stress-related phase transformation. These two properties will be discussed in details.

2.3.1 Shape memory effect

Shape memory alloys show SME when undergoing a deformation while under loading in the twinned martensitic phase (at low temperature) and then the load is removed under austenite finish temperature. The SMA will then recover its initial shape when

the temperature of the material is raised above the austenite finish temperature by phase transition from de-twinned martensite phase to austenite phase. Basically, the SME is a property based on the martensitic phase transition and reorientatiton of martensite variants that occurs without diffusion.

The material starts from a specific starting temperature and a non-loading composition. The SME occurs at relatively low temperatures and therefore the microstructure is initially twinned martensite. The deformation behavior of the material, as a result of the increased loading, is firstly elastic with linear increasing stress (between 1-2), then plastic with almost constant stress(between 2-3), and finally the elastic again with linear increasing stress after the material deformation reaches saturation (between 3-4). Upon removal of the loading (5), residual deformation which we can recover by heating the material to austenite finish temperature with zero load (between 6-7) will be occurred. Finally, the material returns to its initial shape cooling the material to its initial temperature, completely eliminating the deformation.

During loading, the reorientation of the martensite variants that cause observable deformation (between 2-3) starts with the applied stress reaching the critical value for de-twinning (2). Later, the microstructure of the material turns into a fully de-twinned martensite phase, and this phase shows elastic behavior with increasing stress value (between 3-4). During unloading, the material preserves its de-twinned microstructure and the deformation (5). The SMA is heated above the austenite finish temperature to recover obervable deformation, and at the same time, the microstructure of the material transitions from the de-twinned martensitic phase to the austenite phase (between 6-7). Without loading, the microstructure transitions form austenite phase to twinned martensitic phase when while the material is cooling and whole deformation becomes recovered (between 7-1). There is a graphical description that project the state of stress, strain and temperature in Figure 2.3.

The SME that described until now is named one-way SME. In this type of SME, material remembers only the shape on the high temperature. Also, SMAs exhibits the property which is gained by cyclic thermal loading named two-way SME [22]. In this context, the shape memory material remembers the shape in both martensitic phase and austenitic phase. This means that the shape memory material can remember its shape when it is in cold and hot states. With this two-way SME, material can change

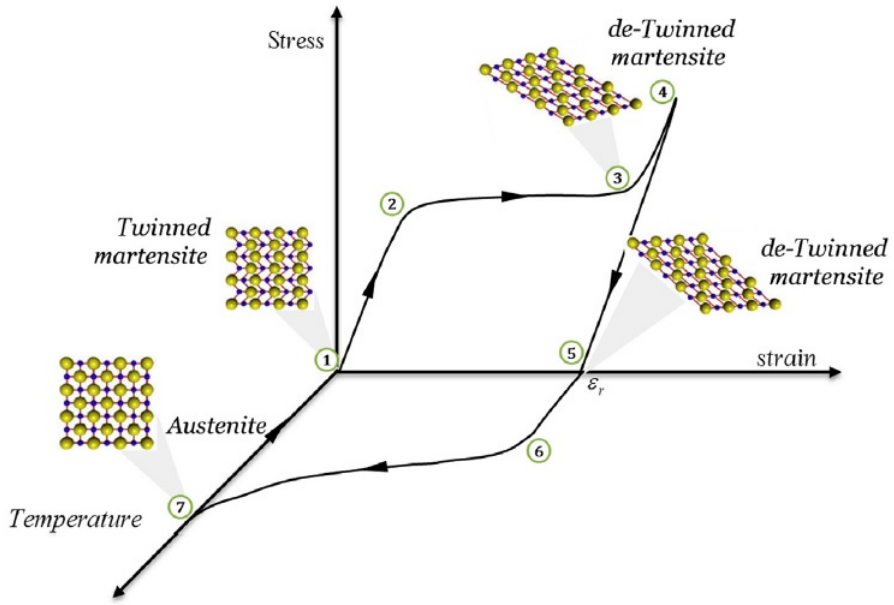

Figure 2.3 : Shape Memory Effect [20].

the shape by heating or cooling without any loadings. The graphical description of two-way SME is in Figure 2.4.

One of the points to take into consideration is that the two-way SME needs to be excited by special process like thermal cycling while the one-way SME is natural behavior of SMAs. To change the temperature of the SMA, the methods of changing the environment temperature or heating the shape memory material with electric current can be used. The SMAs can be used as sensors or actuators which are produce big outputs with small inputs and sizes. In addition, SMA systems are simple enough to consist of only a single spring or a piece of rod or wire.

2.3.2 Superelasticity

The SMA materials can produce high stresses when they activated by heating in some restricted situations. The reverse phase transformation starts and recovery stress is generated in the material that causes it tries to recover its initial shape when the SMA deforms at low temperature and is then externally constrained, as the temperature rises. The shape memory material crystal structure turns into de-twinned martensite and the recovery stress is released upon cooling and when the stress is applied. Then, the original shape is recovered.

The superelastic effect is based on the absence of potential energy in the material and assumed isothermal. The superelasticity is related to absence of stress-induced

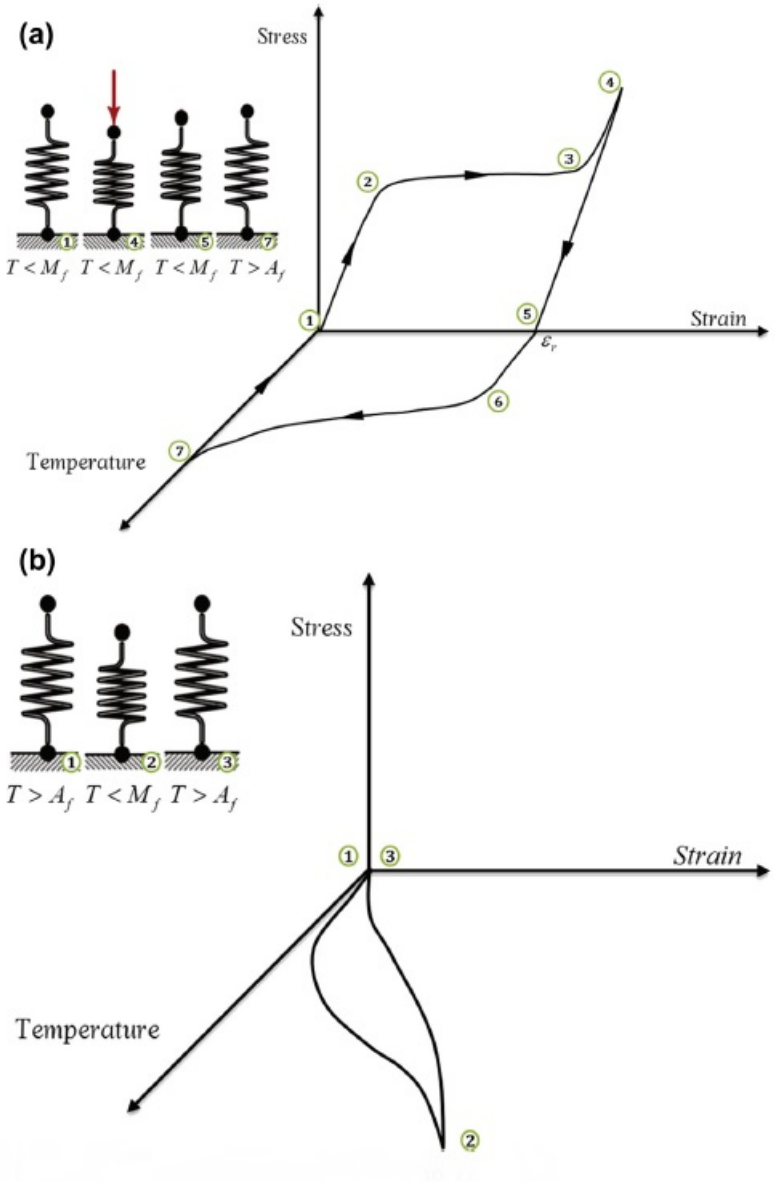

Figure 2.4 : (a)One-way SME and (b)Two-way SME [20].

transformation that causes deformation of the material upon loading and then, shape recovery of the material upon unloading at above the temperatures of austenite finish temperature. The superelasticity process starts at above the austenite finish temperature which the material is in the austenite phase, then proceeds which the material crystal structure becomes de-twinned martensite under the applied load and finally turns back to initial conditions which is austenitic phase and original shape under no stress. The graphical description of superelasticity in stress-strain is in Figure 2.5.

Initially, the shape memory alloy's crystal structure is in the austenitic phase (1). The critical stress which is needed for phase transformation is achieved upon loading (2) and the transformation is completed with de-twinned martensitic phase is gained

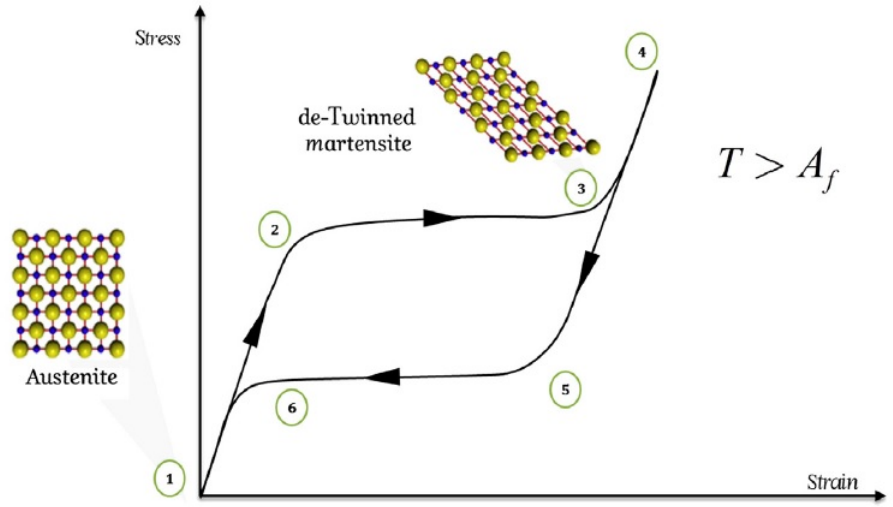

Figure 2.5 : Superelasticity [20].

(between 2-3). Increasing the loading after this point (3) only causes elastic deformation with no change in the crystal structure (between 3-4). Upon unloading, firstly the critical stress for reverse transformation is achieved (5) and the deformed shape is recovered to materials' original shape. Also, the austenite crystal structure is returned which is at the high temperature an no stress (between 4-5-6-1). The superelasticity comes from the hysteresis loop in the stress-strain diagram for SMA.

2.4 Modeling of Shape Memory Alloy

In this section, the SMA model which is used in this thesis is represented. The modeling of 1D behavior, constitutive behavior and the kinetics of phase transition of SMAs and also modification of normal stress-strain behavior to shear stress-strain behavior for modeling of helical spring are described based on the phenomenological studies represented by ref.s [7], [8], [9], [11] and [10]. This is the approach which assumes that there is a linear algebraic relation between the martensite fraction (ξ) and the thermomechanical state variables of SMAs. 1D models can be useful in defining the specific features of the thermomechanical behaviors of the SMAs. Superelasticity, SMEs, reorientation and phase transitions, different properties in different phases are the examples of the 1D models of SMAs including material properties.

2.4.1 Shape memory alloy constitutive models

Various structural models have been proposed that aim to predict the complex thermomechanical behavior of SMAs. Among these models, structural models with external and internal state variables are mostly used. The phase transformation of the SMA material includes the composition of these external and internal variables. An extra internal variable can also be added, representing the martensite fraction, which is considers hardening laws for improving the internal variable upon phase transformation, in the SMA material.

In this section, a few 1D SMA models derived and presented in the researches are briefly mentioned. In ref. [7] has developed a 1D SMA model based on an exponential hardening rules and an internal variable called martensite ratio, which is assumed to have constant material properties during phase transitions. This model does not distinguish between twinned and de-twinned martensite phase. In ref. [8] presented a model that is more adapted to experimental data, defined by the phase transition kinetic rules given by a cosine-based function of the development of the martensite ratio as an internal variable. They accepted the material properties as constant during the phase transitions such as elastic module. By developing Liang's model, in ref. [7] which is used in this thesis offered a model based on the existence of two different internal variables to indicate the ratio of twinned and non-twinned martensite. In this model, the evolution of internal variables is based on a cosine hardening law. Also, in contrast to Liang's model, it contains a variable elastic stiffness during phase transformations.

2.4.2 Shape memory alloy model of Brinson

In ref. [8] explain the de-twinned martensite formation with the model they developed even if no stress is applied. This model offers a useful simplification and approach for using in the applications of SMA materials. In ref. [7] state that three state variables are required to define the composition of SMAs. These are ξ for the martensite ratio, where the alloy is ξ=1 in the case of full martensite and ξ=0 in the case of full austenite; σ for stress; and T for temperature. This relation can be written as,

$$\sigma - \sigma_0 = E(\varepsilon - \varepsilon_0) + \Omega(\xi - \xi_0) + \Theta(T - T_0) \tag{2.1}$$

where σ is the mechanical stress, E is the elastic modulus, ε is the strain, Ω is the phase transformation factor, ξ is the martensitic fraction, Θ is the thermal expansion coefficient, T is the SMA material temperature and the terms with 0 subscript are initial state values.

Brinson model expands the Liang and Rogers model separating the total martensite fraction into the sum of the two different terms,

$$\xi = \xi_t + \xi_d \tag{2.2}$$

where ξ_t is the twinned martensite fraction and ξ_d is the de-twinned martensite fraction. Also, Brinson takes into consideration the martensite fraction dependent terms such as martensite fraction dependent elastic modulus $E(\xi)$ which was mentioned in ref.s [7], [8] and the martensite fraction dependent transformation factor $\Omega(\xi)$. The thermal expansion coefficient is not expressed in terms of martensite fraction because of the small values on the order of five or more. Due to the not considered the temperature-induced phase transformation (twinned martensite), ξ_t assumed as zero in this thesis. Therefore, ξ_d equals ξ.

So, Eq. 2.1 can be written again as,

$$\sigma - \sigma_0 = E(\xi)\varepsilon - E(\xi_0)\varepsilon_0 + \Omega(\xi)\xi - \Omega(\xi_0)\xi_0 + \Theta(T - T_0) \tag{2.3}$$

where $E(\xi)$ is the martensite fraction dependent elastic modulus, $\Omega(\xi)$ is the martensite fraction dependent transformation factor.

A good approximation to represent the martensitic fraction for forward phase transformation (A $\rightarrow$ M) due to the mechanical loading described as cosine function given by Brinson (1993) as,

$$\xi = \frac{1 - \xi_0}{2} \cos\left(\frac{\pi[\sigma - \sigma_f^M]}{\sigma_s^{min} - \sigma_f^{min}}\right) + \frac{1 + \xi_0}{2} \tag{2.4}$$

when $\sigma_s^M < \sigma < \sigma_f^M$. These critical stresses can be written as,

$$\sigma_s^M = \sigma_s^{min} + C_M(T - M_s) \tag{2.5}$$

$$\sigma_f^M = \sigma_f^{min} + C_M(T - M_f) \tag{2.6}$$

Also, the martensitic fraction for reverse phase transformation (M $\rightarrow$ A) due to the mechanical loading as,

$$\xi = \frac{\xi_0}{2}\cos\left(\frac{\pi}{A_f - A_s}\left(T - A_s - \frac{\sigma}{C_A}\right)\right) + 1 \tag{2.7}$$

when $\sigma_s^A > \sigma > \sigma_f^A$. These critical stresses can be written as,

$$\sigma_s^A = C_A(T - A_s) \tag{2.8}$$

$$\sigma_f^A = C_A(T - A_s) \tag{2.9}$$

where C_A and C_M is the material constant associated with critical stresses, which varies depending on the temperature of the material for reverse and forward phase transformation respectively.

2.5 Modeling of Shape Memory Alloy Helical Springs

A SMA helical spring is designed according to SMA constitutive model presented by ref.s [10], [8] and [11] in this section. In this work, normal stresses and strains converted to shear stresses and strains with pure shear approximation which means there is no normal stress or strains. Also, these models that mentioned above are used to reveal nonlinear behaviors of SMA springs. Then, this spring model will be used in aeroelastic model.

2.5.1 Pure shear approximation

The pure shear approximation is considered in this work presented by ref. [10] for modeling of SMA spring. Then, the constitutive relation updated in terms of shear terms with simplified von Mises equation for pure shear related to shear and normal stresses which is $\sigma = \sqrt{3}\tau$, as well as critical stresses. When the same steps is applied to the updated constitutive relation, Eq. 2.3 can be rewritten as,

$$\tau - \tau_0 = G(\xi)\gamma - G(\xi_0)\gamma_0 + \overline{\Omega}(\xi)\xi - \overline{\Omega}(\xi_0)\xi_0 + \overline{\Theta}(T - T_0) \tag{2.10}$$

where τ is the shear stress, $G(\xi)$ is the martensite fraction dependent shear modulus, γ is the shear strain, $\overline{\Omega}(\xi)$ is the transformation strain factor, $\overline{\Theta}$ is the thermal coefficient with respect to shear approximation.

The elastic modulus can differ from phase to phase, such as stress-induced martensitic phase or austenitic phase. These elastic moduluses and martensite fraction relation for a phase state of SMAs is can be written as,

$$E(\xi) = E_A + \xi(E_M - E_A) \tag{2.11}$$

where E_A is austenitic elastic modulus when $\xi = 0$ (entirely austenitic phase) and E_M is martensitic elastic modulus when $\xi = 1$ (entirely martensitic phase). Besides, the relation between shear modulus and elastic modulus can be written as,

$$G(\xi) = \frac{E(\xi)}{2(1+\mu_p)} \tag{2.12}$$

where μ_p is the Poisson's ratio. Then, substituting Eq. 2.11 into Eq. 2.12, the following can be obtained,

$$G(\xi) = \frac{E_A + \xi(E_M - E_A)}{2(1+\mu_p)} \tag{2.13}$$

In addition, the transformation strain factor given as,

$$\overline{\Omega}(\xi) = -G(\xi)\varepsilon_{res} \tag{2.14}$$

where ε_{res} is the maximum residual strain of SMA.

2.5.2 Shape memory alloy spring design

In ref. [11] submitted a conventional spring design with utilizing from a mechanical design textbook presented by Shigley (1977) which can be found in literature. The shear stress of the spring can be expressed as,

$$\tau = \frac{2FR}{\pi r^3} \tag{2.15}$$

where F is the force applied to the spring, R is the spring coil radius, r is the spring wire radius. The small piece cutten from the spring wire, dx, can be seen in Figure 2.6. When a force apply to the spring, the deflection can be determined from the deformation in length of spring. Because of the deformation, the spring will rotate and a torsion angle appears. This angle can be determined from the Hooke's law for torsion as,

$$\gamma = \frac{\tau}{G} = \frac{2FR}{\pi r^3 G} \tag{2.16}$$

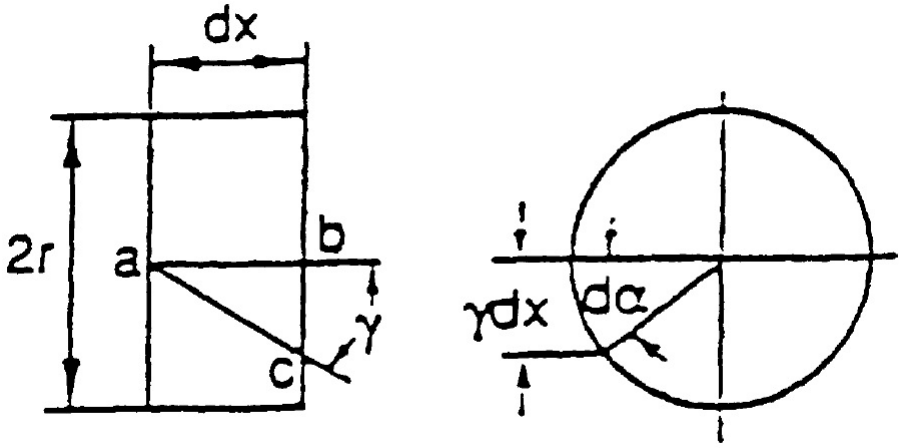

Figure 2.6 : SMA spring small element [11].

The $d\alpha$ angle that one part of the element rotates relative to the other is given by,

$$d\alpha = \frac{\gamma}{r} dx \tag{2.17}$$

Angular deflection of one end of the spring wire accordingly to another is given by,

$$\alpha = \int_0^{2\pi RN} \frac{\gamma}{r} dx = \frac{4FR^2N}{r^4G} \tag{2.18}$$

where N is the amount of SMA spring coils. Therefore, total deflection in the length of spring can be expressed by,

$$y = \alpha R = \frac{4FR^3N}{r^4G} \tag{2.19}$$

Then, the spring constant can be found from the Eq. 2.19 as,

$$k = \frac{F}{y} = \frac{r^4 G}{4R^3 N} \tag{2.20}$$

When considering a SMA spring, Eq. 2.20 can be converted to the following due to the martensite fraction dependent shear modulus as,

$$k(\xi) = \frac{r^4 G(\xi)}{4R^3 N} \tag{2.21}$$

If the initial conditions are assumed as zero ($\tau_0 = \gamma_0 = 0$), SMA is assumed in austenitic phase initially ($\xi_0 = 0$) and the temperature is constant upon process ($T = T_0$), the Eq. 2.10 can be converted to the following as,

$$\tau = G(\xi)\gamma + \overline{\Omega}(\xi)\xi \tag{2.22}$$

and γ can be found from Eq. 2.22 as,

$$\gamma = \frac{\tau - \overline{\Omega}(\xi)\xi}{G(\xi)} \tag{2.23}$$

Thus, if Eq. 2.23 is added in the Eq. 2.18, the angular deflection of the spring converts to,

$$\alpha = \int_0^{2\pi RN} \frac{\frac{\tau - \overline{\Omega}(\xi)\xi}{G(\xi)}}{r} dx = \frac{2\pi RN}{r}\left(\frac{\tau - \overline{\Omega}(\xi)\xi}{G(\xi)}\right) = \frac{2\pi RN}{r}\gamma \tag{2.24}$$

and if Eq. 2.24 is added in the Eq. 2.19, the total deflection in the length of the spring converts to,

$$y = \alpha R = \frac{2\pi R^2 N}{r}\gamma \tag{2.25}$$

In addition, by substituting Eq. 2.15 into Eq. 2.23 and the product into Eq. 2.25, the force related total deflection in the length of the spring equals to,

$$y = \frac{4R^3 N}{r^4 G(\xi)}F - \frac{2\pi R^2 N}{rG(\xi)}\overline{\Omega}(\xi)\xi \tag{2.26}$$

The force of a SMA spring can be found from Eq. 2.27 by arranging the equation as,

$$F^{sma} = \frac{r^4 G(\xi)}{4R^3 NF} y + \frac{\pi r^3}{2R} \overline{\Omega}(\xi)\xi \tag{2.27}$$

Then, by rearranging the Eq. 2.28 and writing the simplified forms we obtain,

$$F^{sma} = k(\xi)y + Y(\xi) \tag{2.28}$$

3. AEROELASTIC AIRFOIL SECTION MODEL WITH SMA SPRING

In this section, aeroelastic problems such as flutter and limit cycle oscillations are discussed. The flutter analysis of two dimensional airfoil section to obtain the boundaries of dynamic instabilities and to suppress these boundaries to LCOs will considered. The solution procedure is based on analytical approaches which make use of unsteady aerodynamic theory. To do this, a simple two degrees of freedom model is considered. This model involves pitch and plunge springs to demonstrate the airfoil motions when airfoil experienced an airflow expressed as α (pitch displacement), h (plunge displacement) and U_∞ (airflow speed) respectively. The pitch and plunge displacements can be measured at the elastic axis which is denoted by e.a.. In this model, the locations of the elastic axis, aerodynamic center which is denoted by a.c. and the center of gravity which is denoted by CG are on the chord line which is denoted by c. The semi-chord length is denoted by b. Distances between the elastic axis and the center of gravity which is denoted by dimensionless x_α and elastic axis and semi-chord which is denoted by dimensionless a are expressed in terms of b and when these parameters are zero, the points lie on the mid-chord position, and when they are positive (negative), the points lie toward the trailing (leading) edge. Then, the stiffnesses of pitch and plunge springs per unit span length (l) are denoted by k_α and k_h respectively. Similarly, the damping coefficients of pitch and plunge springs per unit span length are denoted by d_α and d_h respectively. The aerodynamic lift which is denoted by L is on the aerodynamic center and pitching moment which is denoted by M_α is on the elastic axis. The aeroelastic airfoil section that mentioned above is shown in Figure 3.1 [12] [13].

Generally, the aerodynamic center is assumed at the quarter-chord length from the leading edge in subsonic regime. Also, the elastic axis and the aerodynamic center are assumed at the same point (quarter-chord) in this model.

The aim of this thesis is to analyzing the effects of superelastic hysteresis of SMA springs on two degrees of freedom aeroelastic airfoil section. It is based on the general

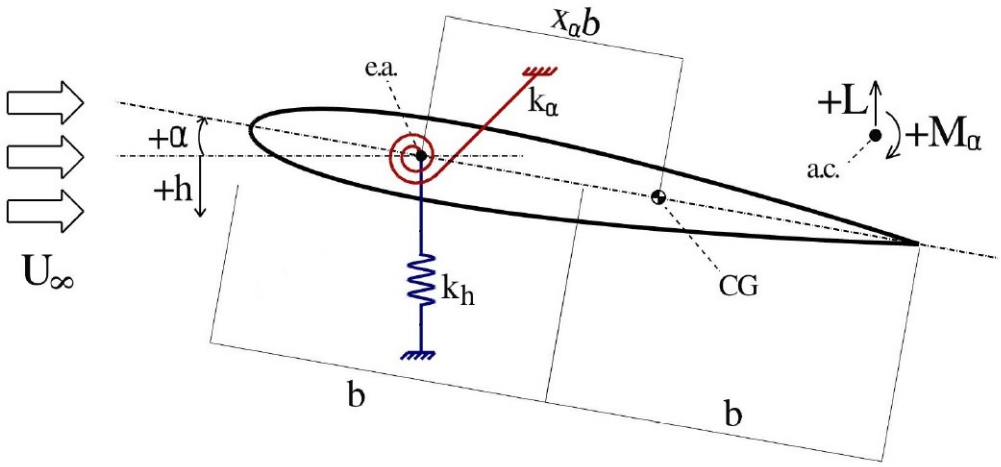

Figure 3.1 : 2 degrees of freedom aeroelastic airfoil section model [23].

aeroelastic behavior of the airfoil section with SMA springs, which will be presented later in the next sections passive control of aeroelastic instabilities is presented. As mentioned earlier, the effects of different preload levels applied to SMA springs and SMA constitutive properties were investigated. Therefore, the two degrees of freedom airfoil section with the derivative SMA springs presented in this section takes into account.

3.1 Equations of Motion of Aeroelastic System

The displacement of a 2 degrees of freedom airfoil that modeled with springs is,

$$\overrightarrow{r} = u\,\overrightarrow{i} + w\,\overrightarrow{k} \tag{3.1}$$

where u is the displacement on the z axis, w is the displacement on the y axis, $\overrightarrow{i}$ and $\overrightarrow{k}$ are the cartesian vector units. We can get from the airfoil section for $\alpha << 1$,

$$u = x(\cos\alpha - 1) \simeq 0 \tag{3.2}$$

$$w = -h - x\sin\alpha \cong -h - x\alpha \tag{3.3}$$

Thus, the kinetic energy can be written as,

$$
\begin{aligned}
T &= \frac{1}{2}\int_{-b}^{b}\left[\left(\frac{dw}{dt}\right)^2+\left(\frac{du}{dt}\right)^2\right]m(x)dx \\
&\simeq \frac{1}{2}\int_{-b}^{b}\left(\frac{dw}{dt}\right)^2 m(x)dx \\
&= \frac{1}{2}\int_{-b}^{b}(-\dot{h}-\dot{\alpha}x)^2 m(x)dx \\
&= \frac{1}{2}\dot{h}^2\int_{-b}^{b}m(x)dx+\frac{1}{2}2\dot{h}\dot{\alpha}\int_{-b}^{b}xm(x)dx+\frac{1}{2}\dot{\alpha}^2\int_{-b}^{b}x^2m(x)dx \\
&= \frac{1}{2}\dot{h}^2 m_t+\frac{1}{2}2\dot{h}\dot{\alpha}S_\alpha+\frac{1}{2}\dot{\alpha}^2 I_\alpha
\end{aligned}
\tag{3.4}
$$

where m_t is the total mass (also equals to $m+m_f$, S_α is the static unbalance (also equals $mx_\alpha b$), I_α is the moment of inertia and $m(x)$ is the mass per unit span. Similarly, the potential energy can be written as,

$$
U = \frac{1}{2}k_h h^2+\frac{1}{2}k_\alpha\alpha^2 \tag{3.5}
$$

where k_α and k_h is the pitch and plunge spring stifnesses respectively. The equations of motion can be obtained by applying the Lagrange equations to the kinetic and potential energy equations. The Lagrange equations is,

$$
\frac{d}{dt}\left(\frac{\partial(T-U)}{\partial\dot{q}_i}\right)-\frac{\partial(T-U)}{\partial q_i}=Q_i \quad i=1,2,... \tag{3.6}
$$

where q_i is the i^th generalized coordinate and Q_i is the i^th generalized force. So, when Lagrange equations are applied to the kinetic and potential energy equations, the followings are obtained as,

$$
\frac{d}{dt}\left(\frac{\partial(T-U)}{\partial\dot{\alpha}_i}\right)-\frac{\partial(T-U)}{\partial\alpha_i}=Q_\alpha \tag{3.7}
$$

$$
\frac{d}{dt}\left(\frac{\partial(T-U)}{\partial\dot{h}_i}\right)-\frac{\partial(T-U)}{\partial h_i}=Q_h \tag{3.8}
$$

and Q_α and Q_h can be obtained as,

$$
\begin{aligned}
\delta W_{NC} &= \delta h\left(-\int Pdx\right)+\delta\alpha\left(-\int Pxdx\right) \\
&= \delta h(Q_h)+\delta\alpha(Q_\alpha) \\
&= \delta h(-L-d_h\dot{h})+\delta\alpha(M_\alpha-d_\alpha\dot{\alpha})
\end{aligned}
\tag{3.9}
$$

So, $Q_h = -L - d_h$ and $Q_\alpha = M_\alpha - d_\alpha \dot{\alpha}$. After all, by taking the time derivatives of Eq.s 3.7 and 3.8, the equations of motions of aeroelastic system can be obtained as,

$$I_\alpha \ddot{\alpha} + m x_\alpha b \ddot{h} + d_\alpha \dot{\alpha} + k_\alpha \alpha = M_\alpha \tag{3.10}$$

$$m x_\alpha b \ddot{\alpha} + (m + m_f)\ddot{h} + d_h \dot{h} + k_h h = -L \tag{3.11}$$

where m is the airfoil mass per unit length, m_f is the fixture mass, M_α is the aerodynamic pitching moment per unit length and L is the aerodynamic lift force per unit length. Also, overdot refers time derivative of terms.

For drawing a comparison between different systems and magnitudes, it is needed to be nondimensionalize the terms in our system. To make the terms in equations of system nondimensional, Eq. 3.10 is divided by mb^2 and Eq. 3.10 is divided by mb. Then, we obtain the followings,

$$r_\alpha^2 \alpha'' + x_\alpha \overline{h}'' + \zeta_\alpha \alpha' + \eta_\alpha^2 r_\alpha^2 \alpha = \overline{M}_\alpha \tag{3.12}$$

$$x_\alpha \alpha'' + \mu \overline{h}'' + \zeta_h \overline{h}' + \overline{h} = -\overline{L} \tag{3.13}$$

where dimensionless time can be expressed as,

$$\bar{t} = \omega_h t$$

the first and second time derivatives of the displacements (α or h) can be given by,

$$\dot{x} = \omega_h x' \qquad \ddot{x} = \omega_h x''$$

where dot (.) refers dimensional time derivative and prime (') refers dimensionless time derivative. Also, r_α is the radius of gyration and given by,

$$r_\alpha = \sqrt{\frac{I_\alpha}{mb^2}} \tag{3.14}$$

ζ_α and ζ_h are pitch and plunge damping ratio respectively and given by,

$$\zeta_\alpha = \frac{d_\alpha}{mb^2\omega_h} \tag{3.15}$$

$$\zeta_h = \frac{d_h}{m\omega_h} \tag{3.16}$$

ω_α, ω_h and η_α are the uncoupled pitch and plunge natural frequencies and frequency ratio respectively and given by,

$$\omega_\alpha = \sqrt{\frac{k_\alpha}{I_\alpha}} \tag{3.17}$$

$$\omega_h = \sqrt{\frac{k_h}{m}} \tag{3.18}$$

$$\eta_\alpha = \frac{\omega_\alpha}{\omega_h} \tag{3.19}$$

$\overline{h} = h/b$ is the dimensionless plunge displacement and the aerodynamic loads $\overline{M}_\alpha$ $-\overline{L}$ can be expressed as,

$$\overline{M}_\alpha = \frac{M_\alpha}{mb^2\omega_h^2} \tag{3.20}$$

$$\overline{L} = \frac{L_\alpha}{mb\omega_h^2} \tag{3.21}$$

Then, the equations of motion in the Eq.s 3.12 and 3.13 can be written in the state space form as,

$$\begin{bmatrix} \mathbf{I} & \mathbf{0} \\ \mathbf{0} & \mathbf{M}_s \end{bmatrix} \begin{Bmatrix} \mathbf{x}_s' \\ \mathbf{x}_s'' \end{Bmatrix} + \begin{bmatrix} \mathbf{0} & -\mathbf{I} \\ \mathbf{K}_s & \mathbf{B}_s \end{bmatrix} \begin{Bmatrix} \mathbf{x}_s \\ \mathbf{x}_s' \end{Bmatrix} = \begin{Bmatrix} \mathbf{0} \\ \mathbf{F} \end{Bmatrix} \tag{3.22}$$

where $\mathbf{I}_{2\times2}$, $\mathbf{0}_{2\times2}$, $\mathbf{M}_s$, $\mathbf{K}_s$ and $\mathbf{B}_s$ are identity, zero, mass, stiffness and damping matrices. $\mathbf{x}_s = \{\alpha \;\; \overline{h}\}^T$ is the displacement state vector and $\mathbf{F} = \{\overline{M}_\alpha \;\; \overline{L}\}^T$ is the aerodynamic load vector. The $\mathbf{M}_s$, $\mathbf{K}_s$ and $\mathbf{B}_s$ matrices can be given as,

$$\mathbf{M}_s = \begin{bmatrix} r_\alpha^2 & x_\alpha \\ x_\alpha & \mu \end{bmatrix} \tag{3.23}$$

$$\mathbf{K}_s = \begin{bmatrix} \eta_\alpha^2 r_\alpha^2 & 0 \\ 0 & 1 \end{bmatrix} \tag{3.24}$$

$$\mathbf{B}_s = \begin{bmatrix} \zeta_\alpha & 0 \\ 0 & \zeta_h \end{bmatrix} \tag{3.25}$$

For defining aerodynamic loads ($\overline{M}_\alpha$ and $\overline{L}$), unsteady aerodynamic model in ref. [24] is used in this thesis. Basically, this work based on the state-space representation of aerodynamic loads, which is useful in numerical analysis, and can be used for arbitrary motions of airfoil in contrast to the Theodorsen (1935) model which is only for harmonic motion. This model can be employed due to the absence of nonlinear behaviour of aeroelastic systems. According to the Theodorsen (1935) model by assuming incompressible flow, the aerodynamic lift and pitching moment can be written as,

$$M_\alpha = -\rho b^2 \left[\pi \left(\frac{1}{2} - a \right) U b \dot{\alpha} + \pi b^2 \left(\frac{1}{8} + a^2 \right) \ddot{\alpha} - \pi b a \ddot{h} \right] + 2\pi\rho U b^2 \left(a + \frac{1}{2} \right) C(\kappa) f(t) \tag{3.26}$$

$$L = -\rho b^2 (U\pi\dot{\alpha} + \pi\ddot{h} - \pi b a \ddot{\alpha}) - 2\pi\rho U b C(\kappa) f(t) \tag{3.27}$$

where U is the airspeed, ρ is the air density, $C(\kappa)$ is generalized Theodorsen function and $f(t)$ is given by [24],

$$f(t) = U\alpha + \dot{h} + b\left(\frac{1}{2} - a \right) \dot{\alpha} \tag{3.28}$$

Theodorsen function ($C(\kappa)$) is a reduced frequency ($\kappa = \omega b/U$) dependent function that represents the effects of vortexes occurring in the trailing edge of airfoil. This reduced frequency refers to the unsteady flow behavior of the air [25]. Due to the classical Wagner function is not useful for numerical analysis, the Jones' (1938) exponential approximation to Wagner function is used in this thesis as [26] [23],

$$\phi(s) = C_0 + C_1 e^{C_3 s} + C_2 e^{C_4 s} \tag{3.29}$$

where $C_0 = 1$, $C_1 = -0.165$, $C_2 = -0.335$, $C_3 = -0.0455$, $C_4 = -0.3$ and $s = Ut/b$. So, the Eq. 3.29 yields,

$$\phi(s) = 1 - 0.165e^{-0.0455s} - 0.335e^{-0.3s} \tag{3.30}$$

According to the ref.s [24] and [23], the $C(\kappa)f(t)$ term in the aerodynamic loads can written with the describing of Duhamel's integral and Pade approximation as,

$$C(\kappa)f(t) = (C_0 + C_1 + C_2)f(t) + C_3C_4(C_1 + C_2)x_{a_1} + (C_1C_3 + C_2C_4)\dot{x}_{a_2} \tag{3.31}$$

where x_{a_1} and $\dot{x}_{a_2}$ are the aerodynamic state terms and they are given by,

$$\dot{\mathbf{x}}_a = \left(\frac{U}{b}\right)\mathbf{S}_1\mathbf{x}_s + \mathbf{S}_2\dot{\mathbf{x}}_s + \left[-C_3C_4\left(\frac{U^2}{b}\right) \quad (C_3 + C_4)\left(\frac{U}{b}\right)\right]\mathbf{x}_a \tag{3.32}$$

where $\mathbf{x}_a = \{x_{a_1} \quad x_{a_2}\}^T$ is the aerodynamic state vector, $\mathbf{S}_1$ and $\mathbf{S}_2$ are the matrices related with the circulatory aerodynamic portion and these are given by,

$$\mathbf{S}_1 = \begin{bmatrix} 1 & 0 \end{bmatrix} \tag{3.33}$$

$$\mathbf{S}_2 = \begin{bmatrix} \left(\frac{1}{2} - a\right) & 1 \end{bmatrix} \tag{3.34}$$

Also, the matrix form of the relation between structural and aerodynamic states as,

$$\mathbf{D} = \frac{1}{\omega_h}\mathbf{R}\mathbf{S}_3 \tag{3.35}$$

where

$$\mathbf{R} = \begin{bmatrix} 2\pi\left(\frac{1}{2} + a\right) \\ -2\pi \end{bmatrix} \tag{3.36}$$

$$\mathbf{S}_3 = \begin{bmatrix} 0.006825\left(\frac{U}{b}\right)^2 & 0.10805\left(\frac{U}{b}\right) \end{bmatrix} \tag{3.37}$$

If derivatives of the Eq.s 3.32 and 3.36 with respect to dimensionless time are included in the Eq. 3.22 and aerodynamic loads are rearranged, the resulting equation can be obtained as,

$$\begin{bmatrix} \mathbf{I} & \mathbf{0} & \mathbf{0} \\ \mathbf{0} & \mathbf{M} & \mathbf{0} \\ \mathbf{0} & \mathbf{0} & \bar{\mathbf{I}} \end{bmatrix} \begin{Bmatrix} \mathbf{x}_s' \\ \mathbf{x}_s'' \\ \mathbf{x}_a' \end{Bmatrix} = \begin{bmatrix} \mathbf{0} & \mathbf{I} & \mathbf{0} \\ -\mathbf{K} & -\mathbf{B} & \mathbf{D} \\ \mathbf{E}_1 & \mathbf{E}_2 & \mathbf{F}_p \end{bmatrix} \begin{Bmatrix} \mathbf{x}_s \\ \mathbf{x}_s' \\ \mathbf{x}_a \end{Bmatrix} \tag{3.38}$$

where $\bar{\mathbf{I}}$ is the induced identity matrix, $\mathbf{M}$ is the mass matrix, $\mathbf{K}$ is the stiffness matrix, $\mathbf{B}$ is the damping matrix which are also have structural and aerodynamic parts all together and these are given by,

$$\bar{\mathbf{I}} = \frac{I}{\omega_h} \tag{3.39}$$

$$\mathbf{M} = \mathbf{M}_s - \frac{\rho b^2}{m}\mathbf{M}_{nc} \tag{3.40}$$

$$\mathbf{K} = \mathbf{K}_s - \frac{\rho b^2}{m}\left(\frac{U}{\omega_h b}\right)^2\left(\mathbf{K}_{nc} + \frac{1}{2}\mathbf{R}\mathbf{S}_1\right) \tag{3.41}$$

$$\mathbf{B} = \mathbf{B}_s - \frac{\rho b^2}{m}\left(\frac{U}{\omega_h b}\right)\left(\mathbf{B}_{nc} + \frac{1}{2}\mathbf{R}\mathbf{S}_2\right) \tag{3.42}$$

where $\mathbf{M}_{nc}$, $\mathbf{K}_{nc}$ and $\mathbf{B}_{nc}$ are noncirculatory aerodynamic mass, stiffness, and damping matrices respectively. Besides, $\mathbf{E}_1$, $\mathbf{E}_2$ and $\mathbf{F}_p$ are are the matrices related with the equations of the aerodynamic model and these are given by,

$$\mathbf{M}_{nc} = \begin{bmatrix} -\pi\left(\frac{1}{8} + a^2\right) & \pi a \\ \pi a & -\pi \end{bmatrix} \tag{3.43}$$

$$\mathbf{K}_{nc} = \begin{bmatrix} 0 & 0 \\ 0 & 0 \end{bmatrix} \tag{3.44}$$

$$\mathbf{B}_{nc} = \begin{bmatrix} \pi\left(-\frac{1}{8} + a\right) & 0 \\ -\pi & 0 \end{bmatrix} \tag{3.45}$$

$$\mathbf{E}_1 = \frac{1}{\omega_h^2}\left(\frac{U}{b}\right)\begin{bmatrix}\mathbf{0}\\ \mathbf{S}_1\end{bmatrix} \tag{3.46}$$

$$\mathbf{E}_2 = \frac{1}{\omega_h}\begin{bmatrix}\mathbf{0}\\ \mathbf{S}_2\end{bmatrix} \tag{3.47}$$

$$\mathbf{F}_p = \frac{1}{\omega_h^2}\begin{bmatrix}0 & 1\\ -0.01365\left(\frac{U}{b}\right)^2 & -0.3455\left(\frac{U}{b}\right)\end{bmatrix} \tag{3.48}$$

The aeroelastic equations of motion can be written as state-space form with the ref. [24] state-space representation of the unsteady aerodynamic model which is convenient for numerical analysis. The Eq. 3.39 can be expressed in the state-space representation and simplified form given as,

$$\mathbf{x}' = \mathbf{A}\mathbf{x} \tag{3.49}$$

where $\mathbf{x} = \{\mathbf{x}_s \quad \mathbf{x}_s' \quad \mathbf{x}_a\}^T$ is the state vector and $\mathbf{A}$ is the state matrix defined as,

$$\mathbf{A} = \begin{bmatrix}\mathbf{0} & \mathbf{I} & \mathbf{0}\\ -\mathbf{M}^{-1}\mathbf{K} & -\mathbf{M}^{-1}\mathbf{B} & \mathbf{M}^{-1}\mathbf{D}\\ \bar{\mathbf{I}}^{-1}\mathbf{E}_1 & \bar{\mathbf{I}}^{-1}\mathbf{E}_2 & \bar{\mathbf{I}}^{-1}\mathbf{F}_p\end{bmatrix} \tag{3.50}$$

3.2 Equations of Motion of Aeroelastic System with Shape Memory Alloy Spring

The aeroelastic airfoil section seen in the Figure 3.2 shows the classical aeroelastic airfoil section with the SMA springs in the pitch degrees of freedom. The pitching spring is replaced by two horizontal SMA springs and one ends of these springs are attached to a massless rigid bar passing through the elastic axis. The distance between the elastic axis and each end of SMA spring is w. The other ends of SMA springs are designed to be fixed only in the pitching degree of freedom but move in the direction of the plunge degree of freedom. Some images, such as plunge springs and abbreviations, have been removed to make the Figure 3.2 clearer.

If equations of motion in Eq.s 3.12 and 3.13 arranged for new aeroelastic airfoil section with SMA spring, the following equations can be obtained as,

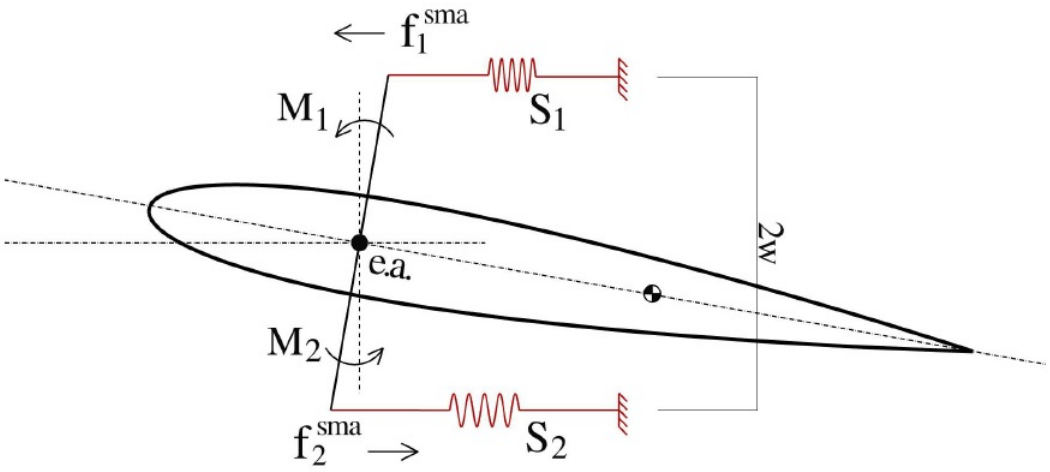

Figure 3.2 : 2 degrees of freedom aeroelastic airfoil section model with SMA spring in the pitch DOF [23].

$$r_\alpha^2\alpha'' + x_\alpha\overline{h}'' + \zeta_\alpha\alpha' + \vartheta(\alpha,\xi_1,\xi_2) = \overline{M}_\alpha \tag{3.51}$$

$$x_\alpha\alpha'' + \mu\overline{h}'' + \zeta_h\overline{h}' + \overline{h} = -\overline{L} \tag{3.52}$$

where $\vartheta(\alpha,\xi_1,\xi_2)$ is the SMA based moment term which replaced with restoring moment term $\eta_\alpha^2 r_\alpha^2\alpha$ in Eq. 3.12 and given by,

$$\vartheta(\alpha,\xi_1,\xi_2) = \frac{w}{mlb^2\omega_h^2}[-F_1^{sma}(\alpha,\xi_1) + F_2^{sma}(\alpha,\xi_2)] \tag{3.53}$$

where $-F_1^{sma}$, $-F_2^{sma}$ and ξ_1, ξ_2 are the force and martensite fraction of SMA springs S_1 and S_2. The distance (w) from each coil spring to the elastic axis may designed to give the same elastic moment values for the model with steel or SMA spring. Thus, below the critical stress values (when no stress-induced phase transformation occurs), the model with steel and SMA spring can be show the same elastic moment values and aeroelastic behavior. So as to get the same elastic moment values, the distance (w) from each coil spring to the elastic axis can be expressed as,

$$w = \sqrt{\frac{k_\alpha l}{2k(\xi)}} \tag{3.54}$$

If the Eq. 2.28 recalled and rearranged for SMA springs variables and displacements, can be expressed as,

$$F_i^{sma}(\alpha,\xi_i) = k(\xi_i)y_i(\alpha) + Y(\xi_i) \quad i = 1,2 \tag{3.55}$$

where $k(\xi)$ is the martensite fraction dependent stiffness of the SMA spring defined in section 2, $y(\alpha)$ is the deflection of the SMA spring in the y axis. The deflection can be expressed as a function of pitch displacements α,

$$y_1(\alpha) = y_0 - w\alpha \tag{3.56}$$

$$y_2(\alpha) = y_0 + w\alpha \tag{3.57}$$

where y_0 is the initial deflection when initially a mechanical preload applied to the springs. Also, $Y(\xi)$ is the effect of the residual strain which occurs along phase transformation and given as,

$$Y(\xi) = -\frac{\pi r^3}{2R} G(\xi)\xi\varepsilon_{res} \tag{3.58}$$

After all, the new version of state-space representation of the aeroelastic model included SMA spring and simplified form can be written as,

$$\mathbf{x}' = \mathbf{A}\mathbf{x} + \mathbf{a}\mathbf{x}_c \tag{3.59}$$

where $\mathbf{x}_c = \{y_1(\alpha) \quad 1 \quad y_1(\alpha) \quad 1 \quad \mathbf{0}\}^T$ is the state vector of SMA springs, $\mathbf{a}$ is the state matrix which included nonlinear effects of SMA springs given by,

$$\mathbf{a} = \begin{bmatrix} \mathbf{0} & \mathbf{0} & \mathbf{0} \\ -\mathbf{M}^{-1}\mathbf{K}_1 & -\mathbf{M}^{-1}\mathbf{K}_2 & \mathbf{0} \\ \mathbf{0} & \mathbf{0} & \mathbf{0} \end{bmatrix} \tag{3.60}$$

where the matrices $\mathbf{K}_i$ are expressed as,

$$\mathbf{K}_i = \frac{w}{mlb^2\omega_h^2} \begin{bmatrix} k(\xi_i) & Y(\xi_i) \\ 0 & 0 \end{bmatrix} \quad i = 1,2 \tag{3.61}$$

If SMA spring is considered, the elastic moment term in the stiffness matrix in Eq. 3.24 should be exported from the matrix and stiffness matrix equals to,

$$\mathbf{K}_s = \begin{bmatrix} 0 & 0 \\ 0 & 1 \end{bmatrix} \tag{3.62}$$

3.3 The Steps and Methods for Shape Memory Alloy State Detection

So far, linear steel spring and SMA springs included aeroelastic models have been described. SMA springs are used in vibration damping applications due to their superelastic properties. These properties are related to phase transformations in their microstructures caused by temperature-induced and/or stress-induced external influences, which also leads to the change in the martensite ratio of the material. As the amount of load applied to the material increases, the phase transformation from austenite to martensite occurs and the martensite fraction increases. Likewise, as the amount of load applied to the material decreases, the phase transformation from martensite to austenite occurs and internal stresses occur. Thus, the martensite fraction decreases assuming $T \geq A_f$. Considering all these relationships and the structural equation, there is a relationship between stress and martensite ratio in co-dependency.

In this section, the martensite fraction of SMAs and stresses can be found only by iterative methods for the above reasons. Since this method will be applied to both SMA springs, no distinction will be made between the two springs. First, pitch displacements will be found step by step using Eq.s 3.56 and 3.57. Then, the shear strains due to the pitch displacements will be found with rewriting the Eq. 2.25 as,

$$\gamma(y_i, \alpha) = \frac{r}{2\pi R^2 N} y_i(\alpha) \tag{3.63}$$

Here, initially it is assumed that the martensite fraction and stress are not known. In other words, the material is initially in the austenitic phase, i.e. $\xi = 0$. Subsequently, relevant shear stresses are found by applying Hooke's law for torsion ($\tau = G\gamma$). However, these stresses found will not be used to calculate instantaneous stress states of SMAs. It will be used to see if SMAs has reached the critical stress level required for phase transformation or not. The stress induced forward phase transformation occurs if,

$$\tau_s^M \leq \tau \leq \tau_f^M \quad and \quad \dot{\xi} > 0 \tag{3.64}$$

and reverse phase transformation occurs if,

$$\tau_s^A \geq \tau \geq \tau_f^A \quad and \quad \dot{\xi} < 0 \tag{3.65}$$

If one of the above conditions is confirmed, the next procedure is to find the corresponding martensite fraction iteratively. If Eq. 3.64 is true, Eq. 2.4 is used to determine the martensite fraction in range between τ_s^M and τ_f^M. If Eq. 3.65 is true, Eq. 2.7 is used to determine the martensite fraction in range between τ_s^A and τ_f^A. Then, these martensite fraction and stress values need to be checked if the Eq. 2.22 satisfy or not. The pair of values that satisfy the constitutive equation will be used to update the next step of the iterative procedure.

If the both Eq.s 3.64 and 3.65 are not true, then no need to make any iterative procedure. SMA behaves like linear steel spring out of these stress ranges.

4. AEROELASTIC AIRFOIL SECTION ANALYSIS WITH SMA SPRING

In this thesis, the models that mentioned above are investigated and analyzed in three section. The first one is shape memory alloy springs' natural and structural behaviors. The second one is the influences of this SMA springs' behaviors on the aeroelastic airfoil section at the flutter condition. The third one is the influences of this SMA springs' behaviors on the aeroelastic airfoil section at the post-flutter condition.

4.1 Code Validation

The codes are generated to find the flutter speed, modal damping and frequencies, SMA spring's structural behaviors and SMA influences on the aeroelastic behavior of system that mentioned above. For the validating this code, a few examples are found from literature and the parameters of this examples are applying in our code.

The first example is a 2 DOF aeroelastic airfoil section problem from the ref. [12]. The properties and nondimensional parameters of this example are given as;

Table 4.1 : Hodges and Pierce (2011) Aeroelastic Parameters.

Parameter	Value	Unit
a	-0.2	-
x_α	0.125	-
μ	20	-
r_α^2	0.24	-
ω_h/ω_α	0.4	-

The flutter speed is found as 1.849 which is closer value in the reference and the results are compared in the Fig. 4.1 with the modal damping and frequencies as;

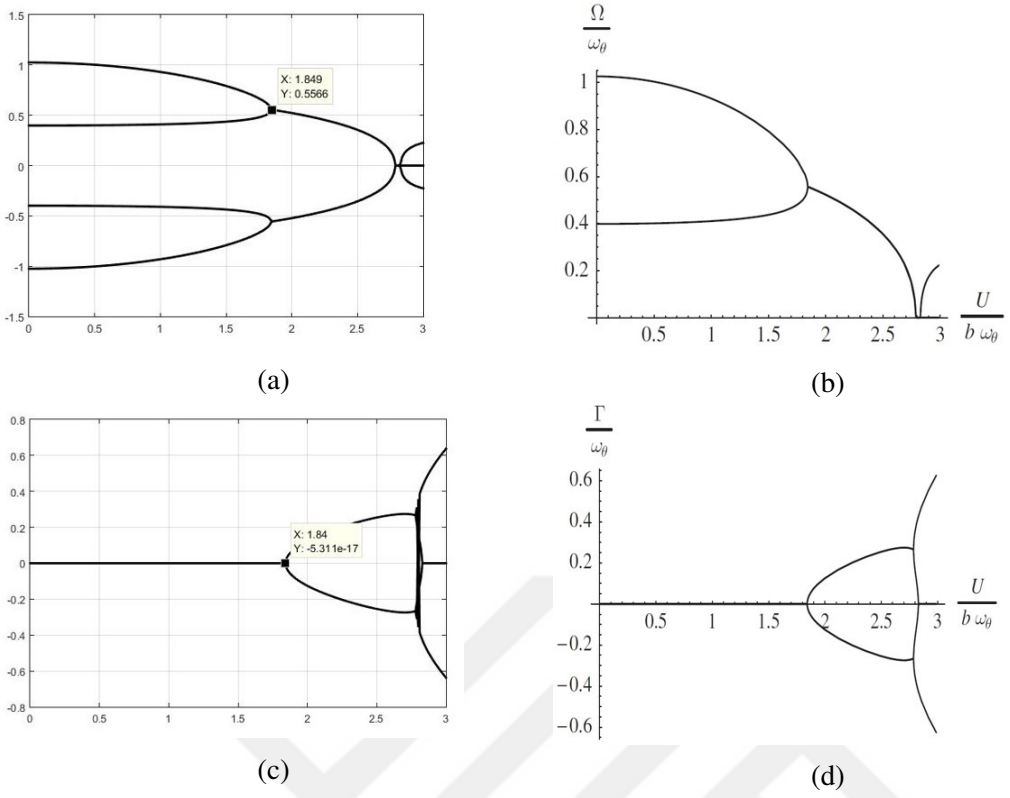

Figure 4.1 : (a) result of my code on modal frequency (b) result of reference on modal frequency (c) result of my code on modal damping (d) result of reference on modal damping.

Other example is again a 2 DOF aeroelastic airfoil section with SMA spring and quasi-steady aerodynamic theory problem from the ref. [17]. The properties and nondimensional parameters of this example are given in Table 4.2;

Table 4.2 : Malher (2015) Aeroelastic Parameters.

Parameter	Value	Unit
a	-0.2	-
x_α	0.2	-
μ	$1/10\pi$	-
r_α	0.5	-
ω_h/ω_α	0.5	-
γ	0.4	-
C_L, α	2π	-

The flutter speed is found as 0.8637 which closer value in the reference and the results are compared in the Fig. 4.2 with the real and imaginary parts of eigenvalues and also the damping effect of SMA spring on the displacements of airfoil section as;

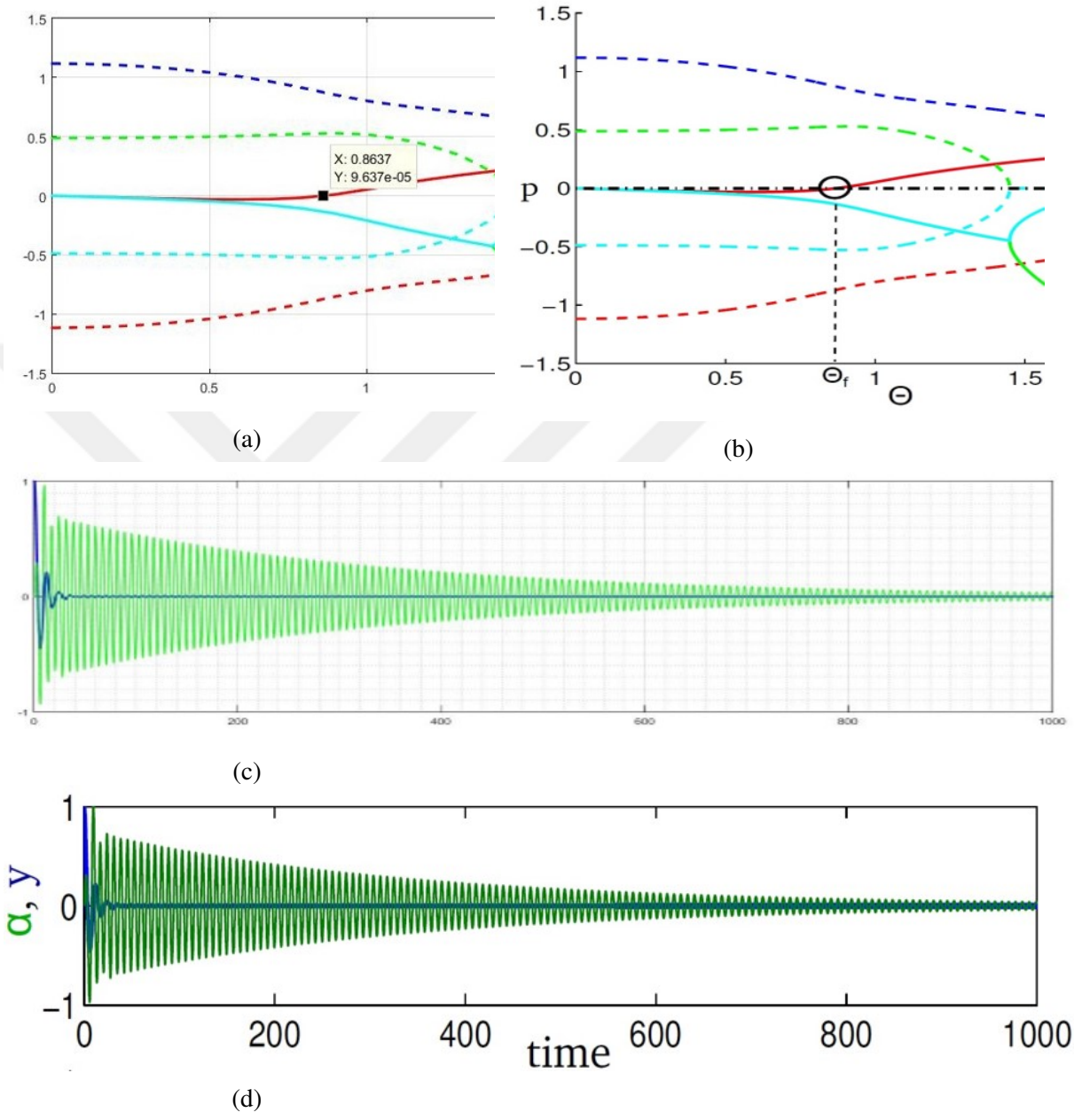

(a) (b)

(c)

(d)

Figure 4.2 : (a) result of my code on eigenvalues (b) result of reference on eigenvalues (c) result of my code on displacements (d) result of reference on displacements.

The last example is again and again a 2 DOF aeroelastic airfoil section with SMA spring and unsteady aerodynamic theory problem from the ref. [18]. The properties and nondimensional parameters of this example are given in Table 4.3 and 4.4. The

flutter speed is found as 11.62 which is closer value in the reference and the results are compared in the Fig. 4.3 with the displacements of airfoil section as;

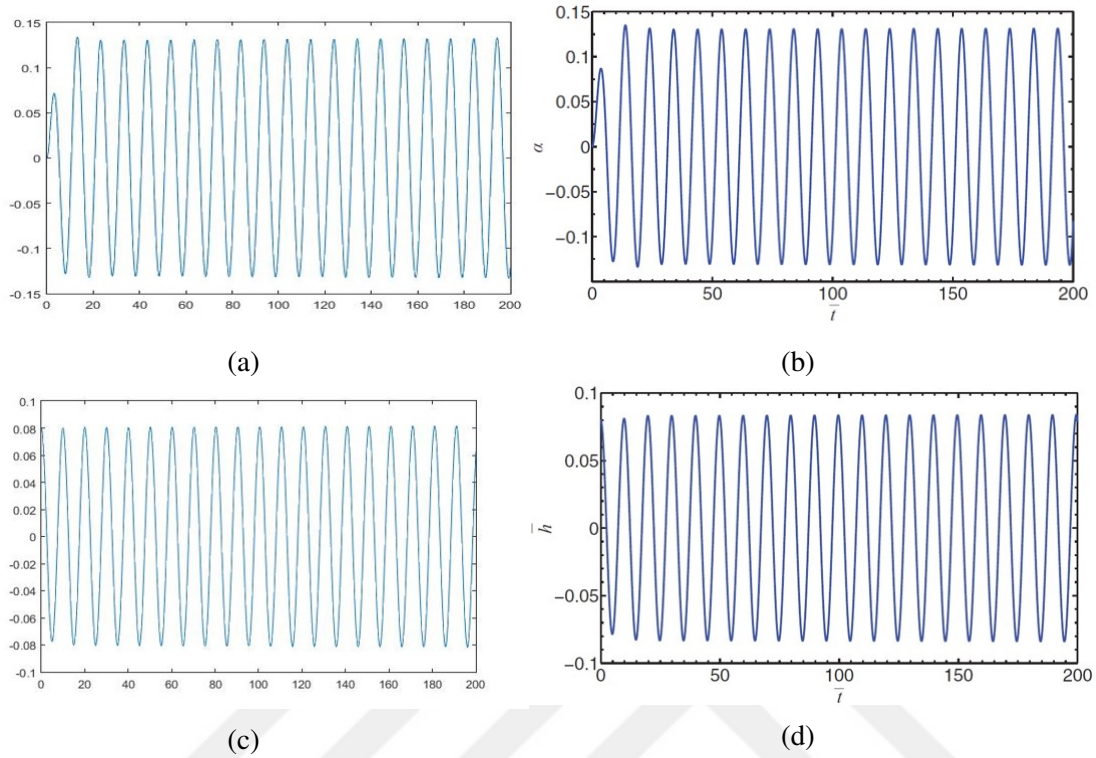

Figure 4.3 : (a) result of my code on pitch dislacements (b) result of refrence on pitch dislacements (c) result of my code on plunge dislacements (d) result of reference on plunge dislacements.

Also, the the error rates of our code results and Sousa (2016) results can be seen on Fig. 4.4 as;

	Dağlı	Sousa	Error rate in %
Max. tension pitch displacement	0,1338	0,13317	0,470852018
Min. compression pitch displacement	-0,1328	-0,13317	-0,278614458
Max. tension plunge displacement	0,0817	0,0822	-0,611995104
Min. compression plunge displacement	-0,0819	-0,0822	-0,366300366
Max. tension shear stress	47,015	47	0,031904711
Min. compression shear stress	-47,347	-47	0,732886983
Flutter speed	11,62	11,6	0,172413793

Figure 4.4 : Comparison of our code and Sousa (2016) with error rate.

4.2 Shape Memory Alloy Springs' Natural and Structural Behaviors

There are two condition when describing SMA material behavior, temperature and stress. In Table 4.3, the SMA parameters which are used along all analyzes in this chapter and these parameters are obtained from Aguiar et al. (2013).

Table 4.3 : Shape Memory Alloy Parameters.

Parameter	Value	Unit
M_f	302	K
M_s	315	K
A_s	316	K
A_f	331	K
C_M	4	MPa/K
C_A	6	MPa/K
σ_s^{min}	100	MPa
σ_f^{min}	170	MPa
ε_{res}	6.7	%
G_M	11.5	GPa
G_A	14.5	GPa
μ_p	0.3	-

The effects of these conditions are previously defined in chapter 2 and can be seen in Fig. 4.5 for the properties above at different temperatures. The forward phase transformation ($M \rightarrow A$) starts when mechanical shear stress reachs to the minimum start stress ($\tau \geq \tau_s^{min}$ where $\tau_s^{min} = \sigma_s^{min}/\sqrt{3}$) and finishes when mechanical shear stress reachs to the minimum finish stress ($\tau \geq \tau_f^{min}$ where $\tau_f^{min} = \sigma_f^{min}/\sqrt{3}$). These critical stresses does not change with increasing temperature until temperature reaches to the M_s temperature. After this temperature, critical stresses increase linearly with increasing temperature.

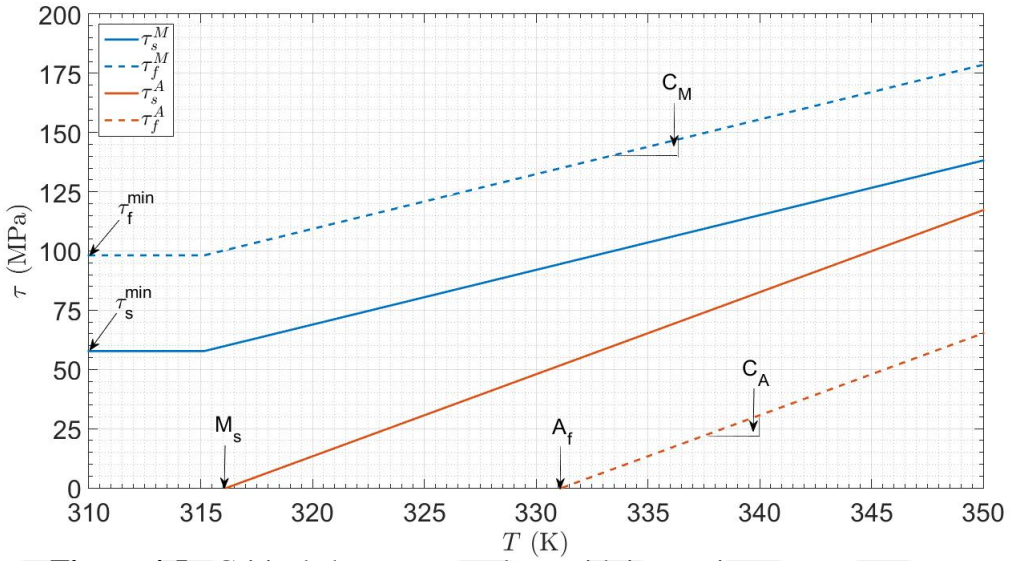

Figure 4.5 : Critical shear stress values with increasing temperature.

Fig.s 4.6 shows the stress-strain graphic of the SMA spring at different temperatures. As seen in the figure, the material exhibits residual strain up to the austenite finish temperature (A_f). This is related to the shape memory effect (SME). After the austenite finish temperature, the material creates hysteresis by showing superelastic behavior and the deformation is completely recovered. As the critical stress values of SMAs increase with increasing temperature, the hysteresis rises and the hysteresis area decreases with increasing temperature.

The phase transformation that is occuring at austenite finish temperature (A_f) represented in Fig. 4.6 (c) is detailing in Fig. 4.7 with the change of martensite fraction and shear modulus by the transformation. In Fig. 4.7 (a) the material is in the fully austenitic phase initially. Then, the martensite fraction increases between τ_s^M and τ_f^M when forward phase transformation occurs and decreases between τ_s^A and τ_f^A when reverse phase transformation occurs. Out of these ranges, the martensite fraction is constant. At the same time, the shear modulus decreases between τ_s^M and τ_f^M and increases between τ_s^A and τ_f^A.

4.3 Aeroelastic Numerical Analysis

Shape memory alloy spring's influences on the aeroelastic airfoil section are analyzed and the results are presented. Aeroelastic airfoil section parameters and spring geometries are given in Table 4.4. The parameters which are used in this analysis

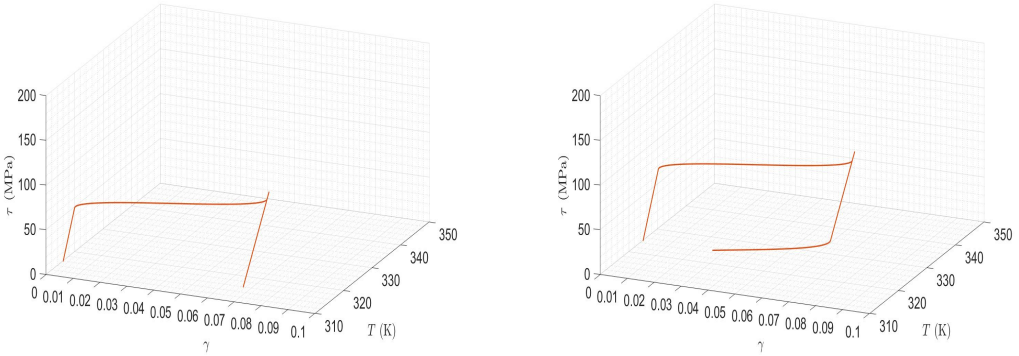

(a) 316 K (b) 325 K

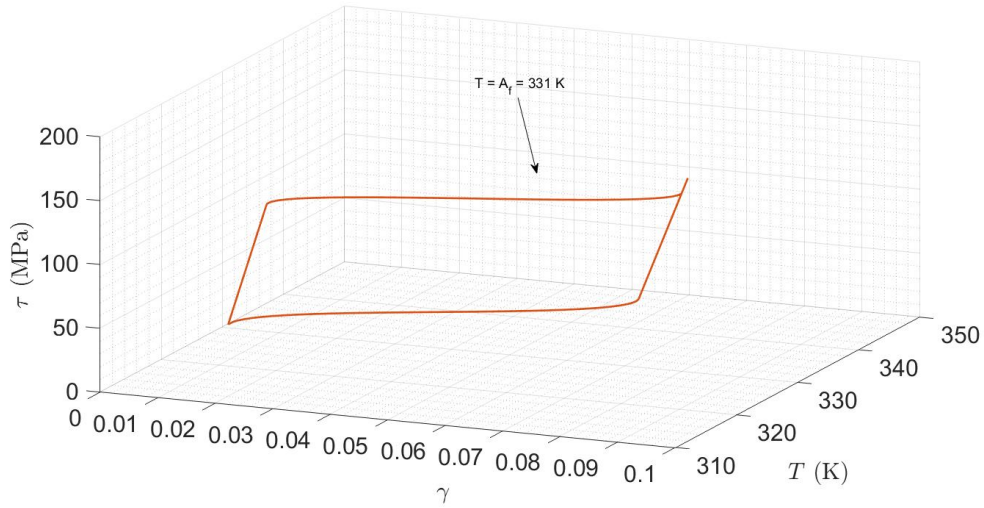

(c) 331 K

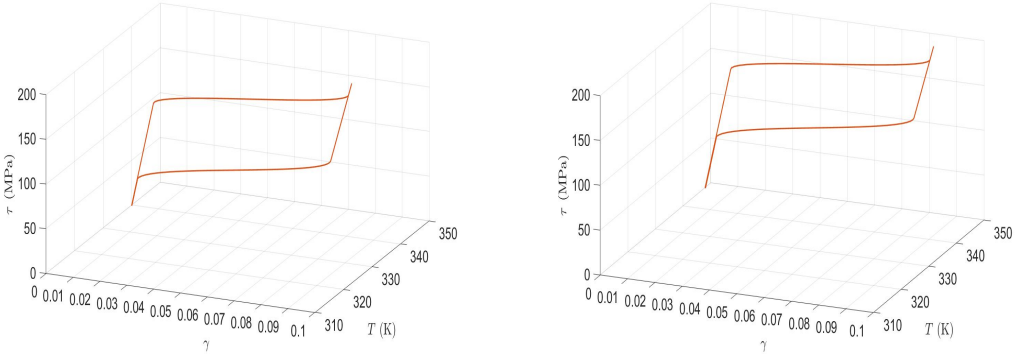

(d) 340 K (e) 348 K

Figure 4.6 : Shear stress - strain graphics for different temperatures.

are taken from ref. [23]. It is important to remember that all analyses of this section are maden at the constant $A_f = 331\ K$, initial condition $\overline{h}_0 = 0.08$ and the material is in the fully austenitic phase initially. The length of SMA spring is $36.7mm$. As a result of this conditions, the stiffness of spring and critical stresses can be found as $k = 174.75\ N/m$, $\tau_s^M = 95\ MPa$, $\tau_f^M = 135\ MPa$, $\tau_s^A = 52\ MPa$ and $\tau_f^A = 0\ MPa$ respectively.

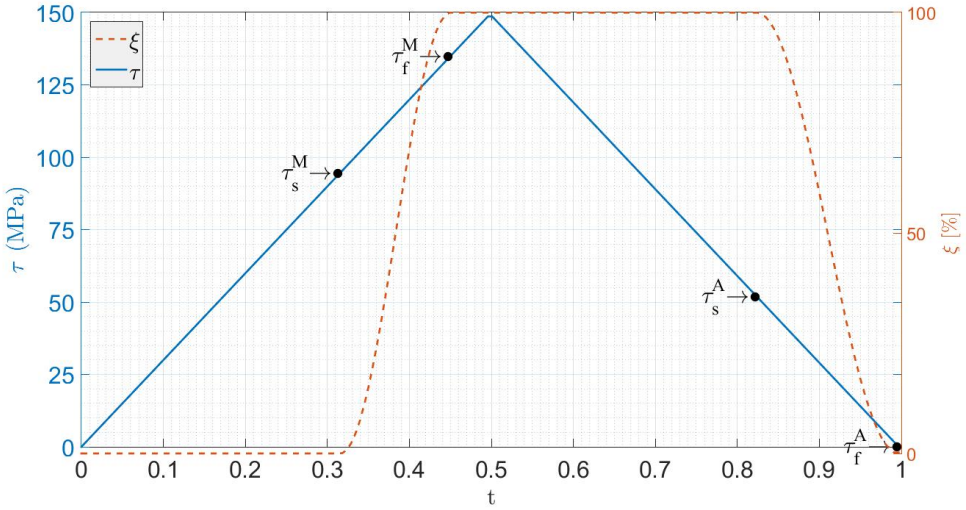

(a)

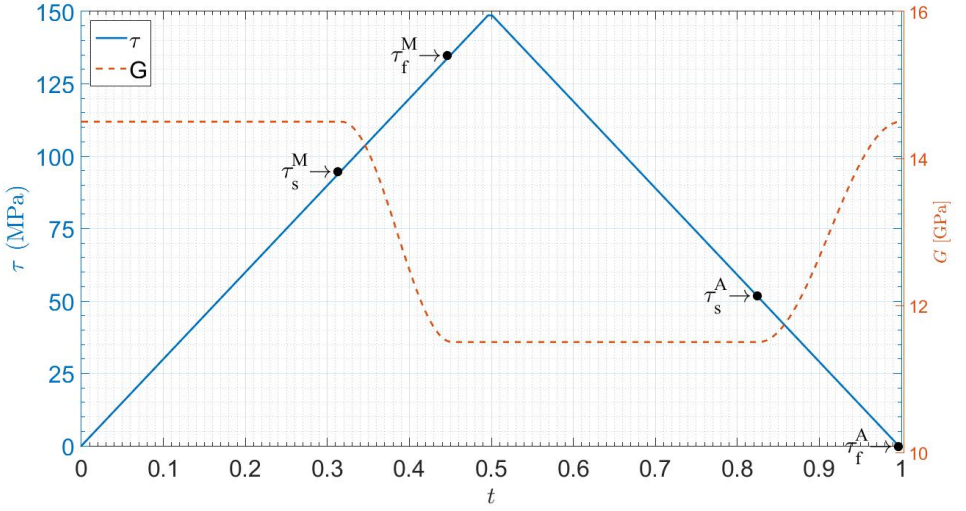

(b)

Figure 4.7 : The change in the material properties with loading-unloading (a) for martensite fraction (b) for shear modulus at A_f.

4.3.1 Analysis at flutter speed

First of all, SMA spring's influences on the aeroelastic airfoil section are analyzed at flutter speed. When an aeroelastic airfoil section considered for flutter, if airspeed does not exceed the flutter speed, the airfoil is stable. If airspeed exceeds the flutter speed, the airfoil is not stable and this may cause a structural failure. The same situation is valid for aeroelastic airfoil section with SMA spring, if no phase transformation occurs. In other words, the SMA spring is behaves like the steel spring when stress values does not reach the critical values.

Table 4.4 : Aeroelastic Airfoil Section Parameters.

Parameter	Value	Unit
l	0.5	m
b	0.125	m
c	-0.5	-
x_α	0.256	-
m	1.542	kg/m
m_f	2.548	kg/m
I_α	0.0072	$kg.m$
k_α	5.08	N/rad
k_h	4200	N/m^2
ζ_α	0.088	-
ζ_h	0.0035	-
w	0.085	m
r	0.00095	m
R	0.008	m
N	16.5	-

The flutter speed, pitch and plunge displacements and shear stress of SMA spring are can be seen in Fig.s 4.8 and 4.9. In Fig. 4.8 (a), one of the real parts of the eigenvalue which crosses at the zero point is shown and the flutter speed is captured from this point as 11.6 m/s. The spring length is stretches maximum 11 mm forward and back and related maximum shear stress is found 47 MPa and can be seen in Fig. 4.8 (b). This maximum stress value is smaller than the minimum shear stress value for phase transformation. So, this aeroelastic airfoil section with SMA spring is shows same behaviors like aeroelastic airfoil section with steel spring. In order to reveal the influences of the SMA spring, needed to exceed the minimum shear stress value. Applying preload to the springs will increase the shear stress value and will exceed the minimum shear stress value. For this reason, by applying a few different preload values to the springs, it will be tried to exceed the minimum shear stress value and to reveal the effects of the SMA spring.

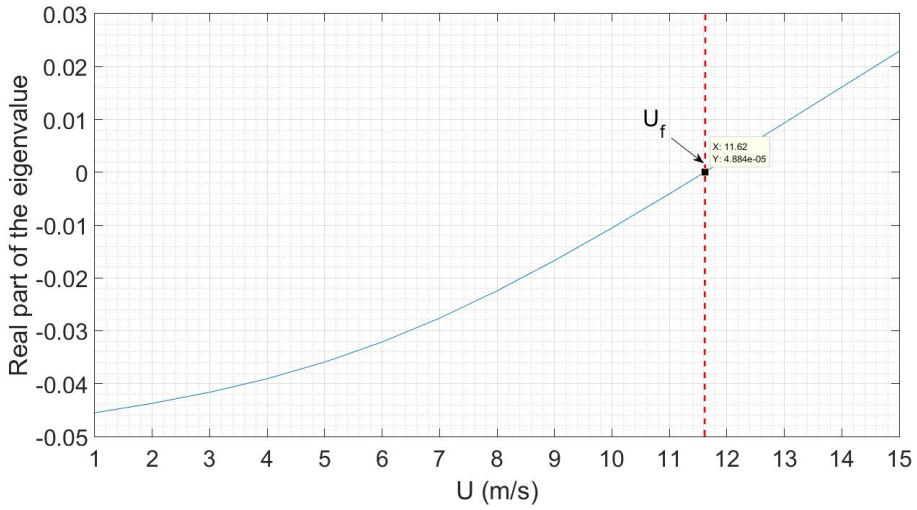

(a)

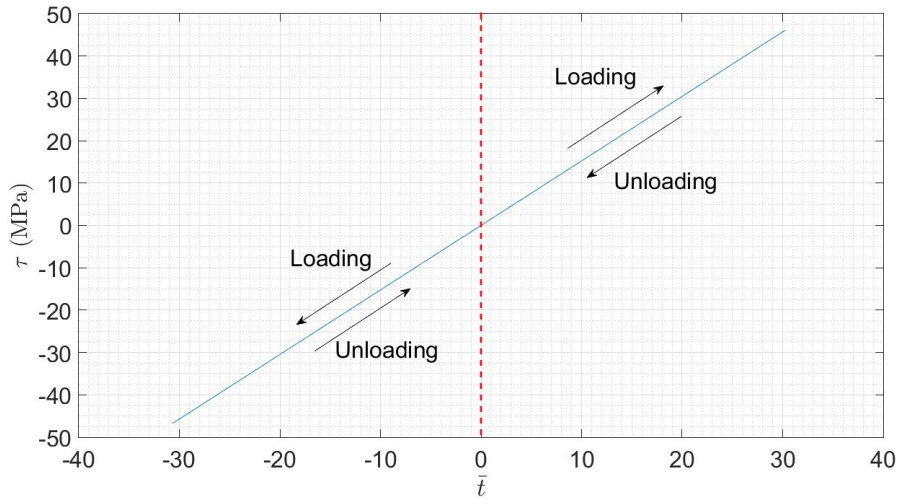

(b)

Figure 4.8 : Flutter prediction and stress behaviors of spring (a) real part with increasing airflow (b) stress with changing stretching.

Different preload values are applied to the springs and the results can be see in Fig. 4.10 to 4.13. As seen in the figures, the pitch and plunge displacements oscillations decreases with increasing preload values due to the SMA spring's nonlinear dissipation effects. After 4.5 N preload value, the pitch and plunge oscillation magnitude falls by half. After a specific preload value, the pitch and plunge oscillation magnitude does not decrease too much as much as at beginning.

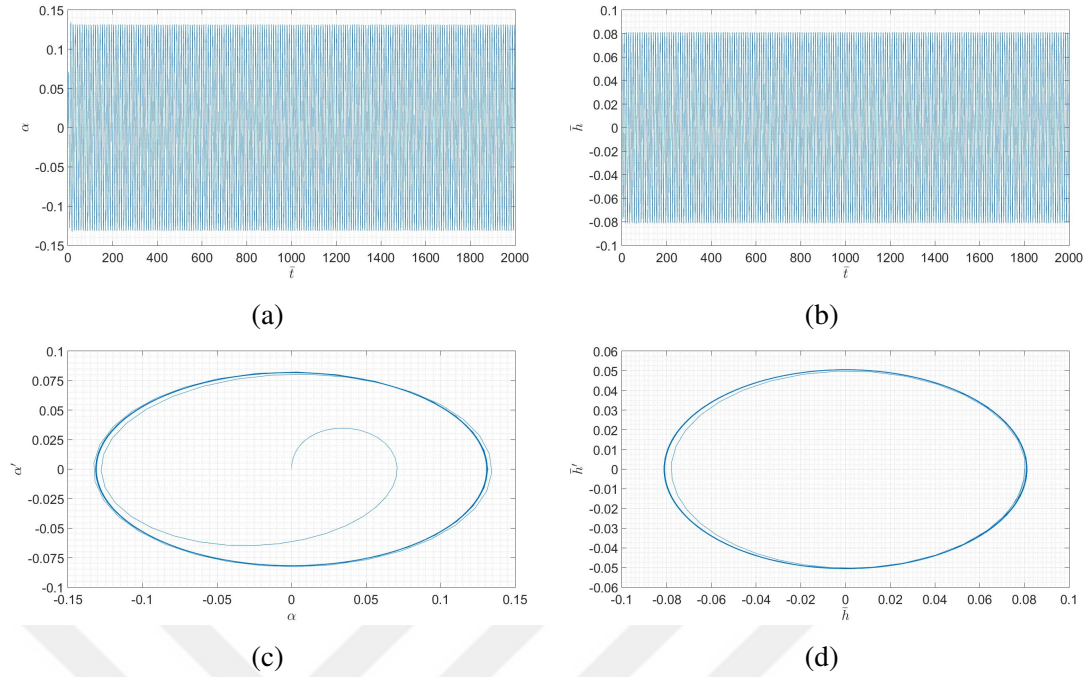

Figure 4.9 : Displacements at flutter speed (a) pitch displacement with dimensionless time (b) plunge displacement with dimensionless time (c) pitch displacement phase portrait (d) plunge displacement phase portrait.

The change of pitch and plunge oscillation according to the amplitudes with increasing preload value are shown in Fig. 4.14 which involves both steel and SMA spring for comparison. As seen in the figure, preload values after 2 N the amplitudes are started to decrease. For the preload values smaller than 2 N, the aeroelastic system shows the same behaviors as in the Fig. 4.10 to 4.13 (a) and (b). Can be easily seen in the figures that linear stable oscillations at flutter speed are turns into the LCOs with incresing preload values. This is because of the damping effect of SMA spring.

In order to see better the damping effect occured by the preloading of the SMA springs, the analysis performed in Fig. 4.15 without preloading and with 3.5 N preloading are compared in the same figure. The comparisons for pitch displacements (a), plunge displacements (b), pitch phase portrait (c) and plunge phase portrait (d) can be seen in Fig. 4.15. Also, the Fig. 4.15 shows that the change of the (e) martensite fraction and (f) stiffness of the SMA spring with dimensionless time for without preloading and with 3.5 N preloading again. The martensite fraction does not reach zero again after the phase transformation starts. Also, SMAs can show different behaviors for different initial conditions.

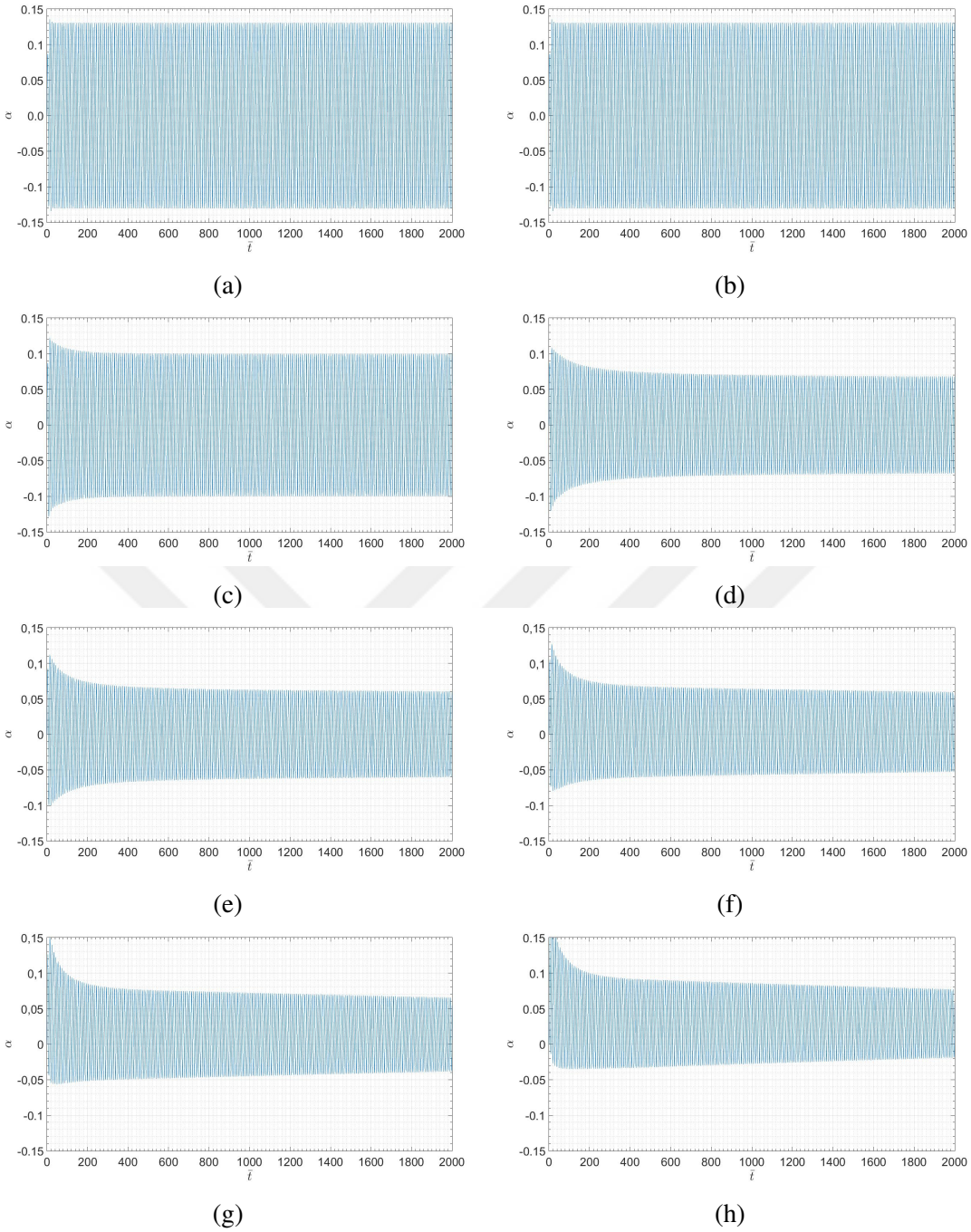

Figure 4.10 : Pitch displacements with different preloads at flutter speed (a) 1 N (b) 2 N (c) 2.5 N (d) 3 N (e) 3.5 N (f) 4 N (g) 4.5 N (h) 5 N.

4.3.2 Analysis at post-flutter speed

Secondly, SMA spring's influences on the aeroelastic airfoil section are analyzed at post-flutter speed. A stable aeroelastic system is shown against small or large disturbances under the flutter boundary provided by a linear dynamic model. Beyond the flutter boundary, LCOs occurs due to some nonlinear effect, and typically the LCOs

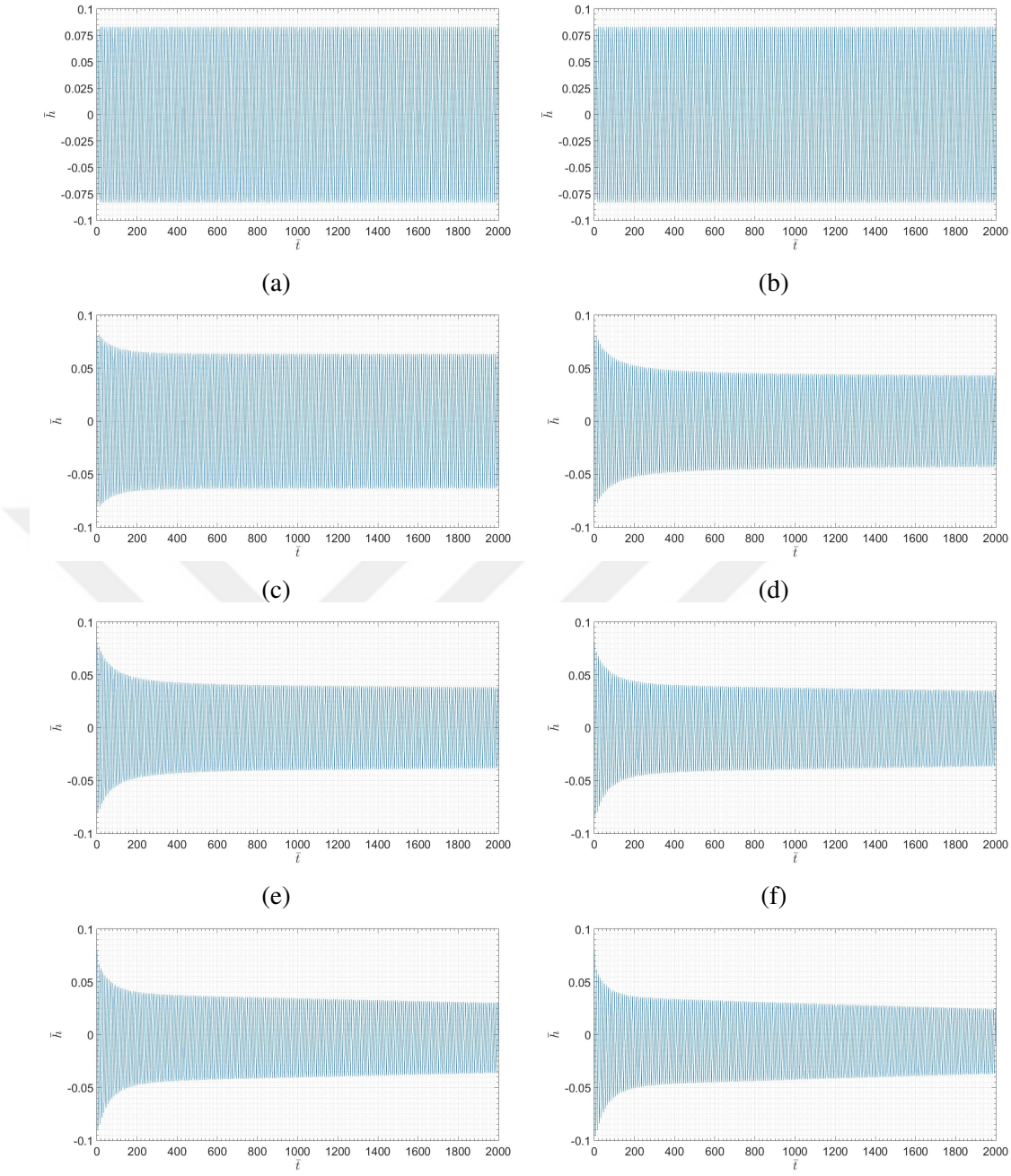

Figure 4.11 : Plunge displacements with different preloads at flutter speed (a) 1 N (b) 2 N (c) 2.5 N (d) 3 N (e) 3.5 N (f) 4 N (g) 4.5 N (h) 5 N.

amplitude increases as the flight speed increases beyond the flutter speed. Another common possibility is that if the disturbances in the system are large enough, LCOs can also be present below the flutter boundary (Dowell, 2015). Converting unstable motions above the flutter speed to LCOs is useful in aeroelastic system for convertable amplitudes by SMA spring nonlinear effect.

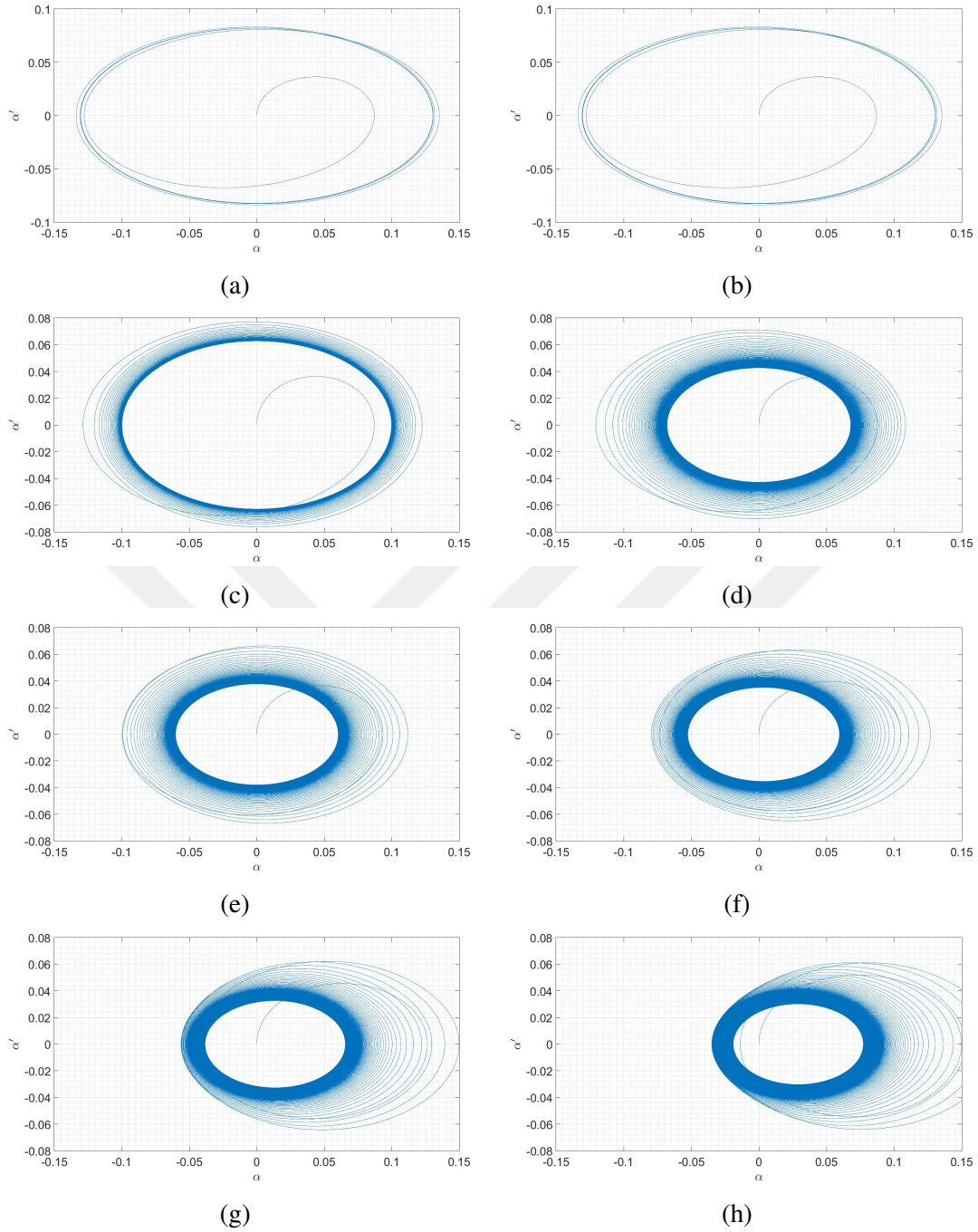

Figure 4.12 : Pitch displacement phase portraits with different preloads at flutter speed (a) 1 N (b) 2 N (c) 2.5 N (d) 3 N (e) 3.5 N (f) 4 N (g) 4.5 N (h) 5 N.

In Fig. 4.16, the nonlinear effects of SMA spring above flutter speed (which is 14 m/s) for 3.5 N preload value and acceptable LCOs can be seen. Fig. 4.16 (a) and (b) shows pitch and plunge displacements with dimensionless time, (c) and (d) shows pitch and plunge displacements phase portraits, (e) and (f) shows the change of martensite fraction and stiffness of SMA spring.

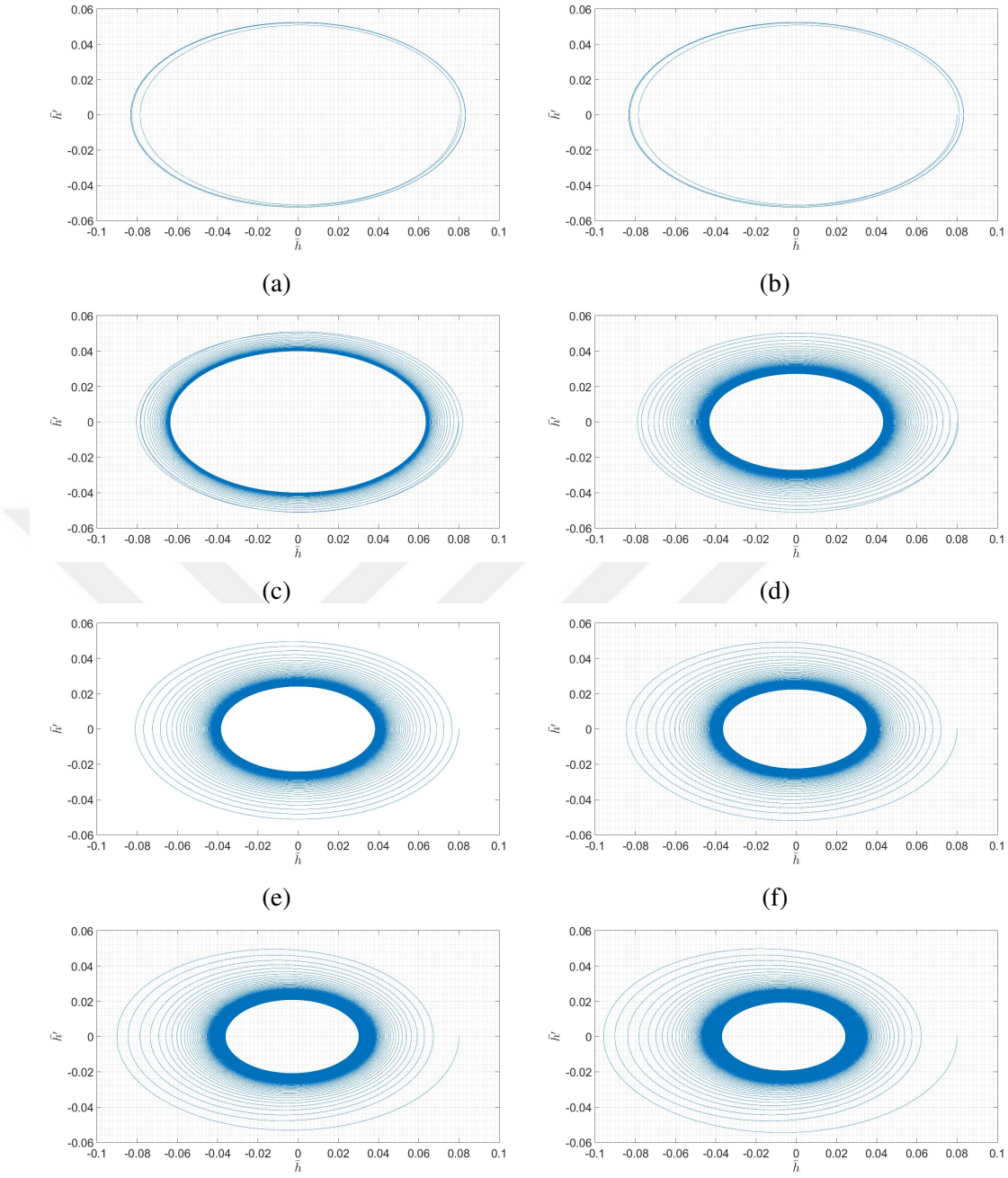

Figure 4.13 : Plunge displacement phase portraits with different preloads at flutter speed (a) 1 N (b) 2 N (c) 2.5 N (d) 3 N (e) 3.5 N (f) 4 N (g) 4.5 N (h) 5 N.

In Fig. 4.17, the minimum and maximum shear stresses which are generated by pitch displacements of SMA springs with increasing preload values for both flutter speed (11.6 m/s, the red area) and post-flutter speed (14 m/s, the blue area). For post-flutter condition, acceptable LCOs should be considered because the low preload values can not absorb the oscillations at high flutter speed. Therefore, the blue area or stress values for post-flutter speeds up to 2 N preload value can not be absorbed

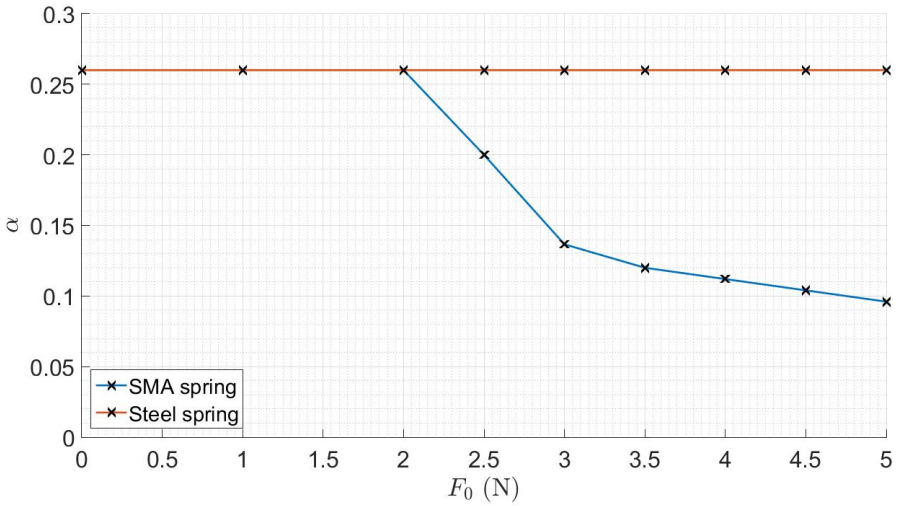

(a)

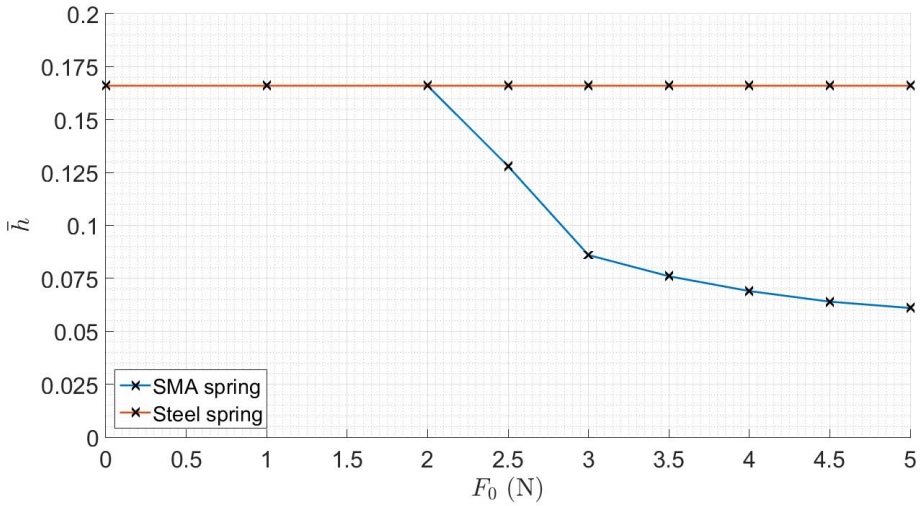

(b)

Figure 4.14 : (a) pitch and (b) plunge amplitudes with increasing preloads.

by SMA springs and not shown in the figure. The maximum values (upper sides of the areas) of the shear stresses can be given by the stress derived from sum of the preload and pitch displacement. Stresses are summed due to the opposite direction of the preload and pitching displacement. Similarly, the minimum values (lower sides of the areas) of the shear stresses can be given by the stress derived from preload minus pitch displacement. For the high preload values, the minimum shear stress values can be derived positive due to that the preload induced stress is bigger than the pitch displacement induced stress. The maximum and minimum values refers to the tensile and compression loadings respectively.

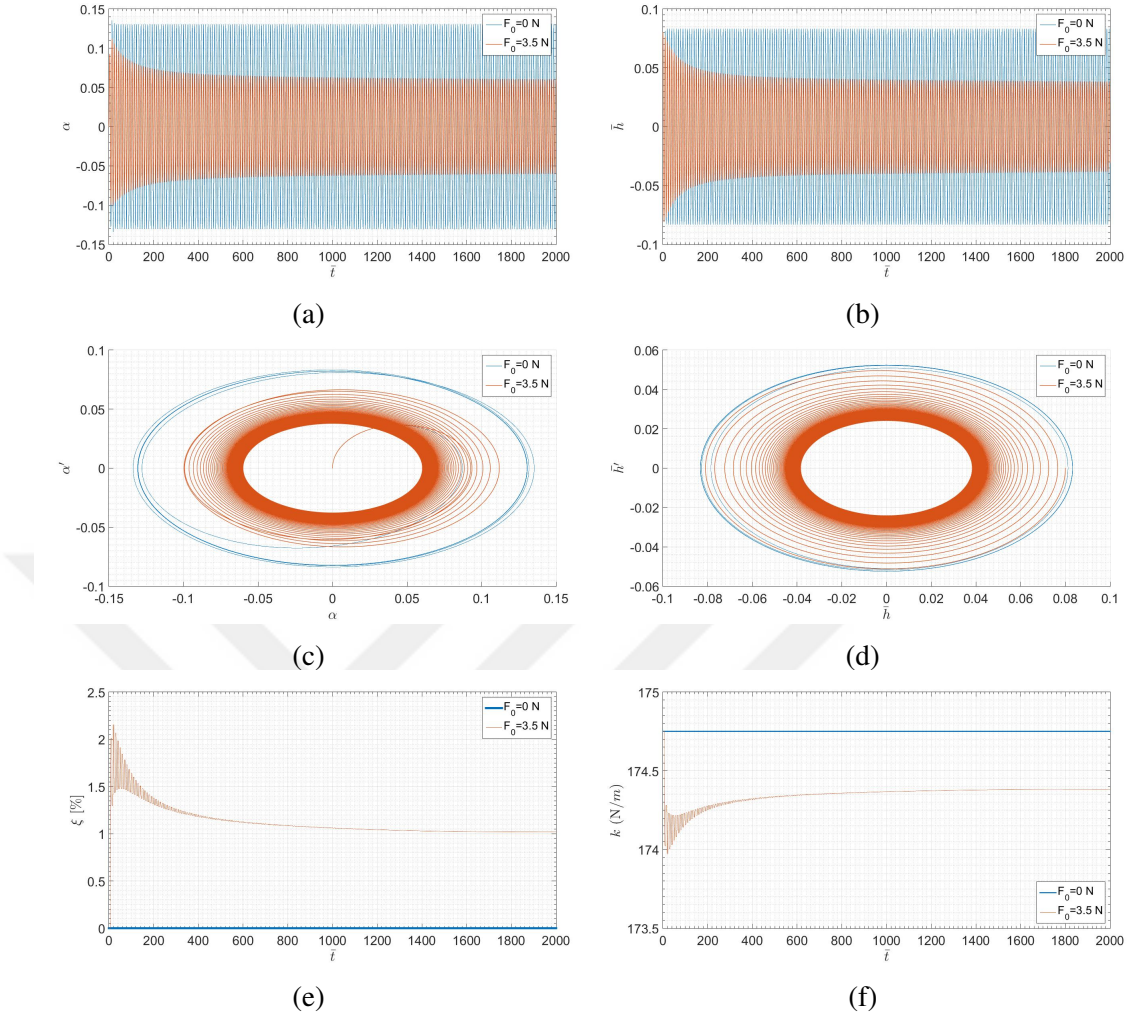

Figure 4.15 : Comparison for 0 N and 3.5 N aeroelastic analysis SMA spring results (a) pitch displacement with dimensionless time (b) plunge displacement with dimensionless time (c) pitch displacement phase portrait (d) plunge displacement phase portrait. Also, the corresponding change in the (e) martensite fraction and (f) stiffness of the spring.

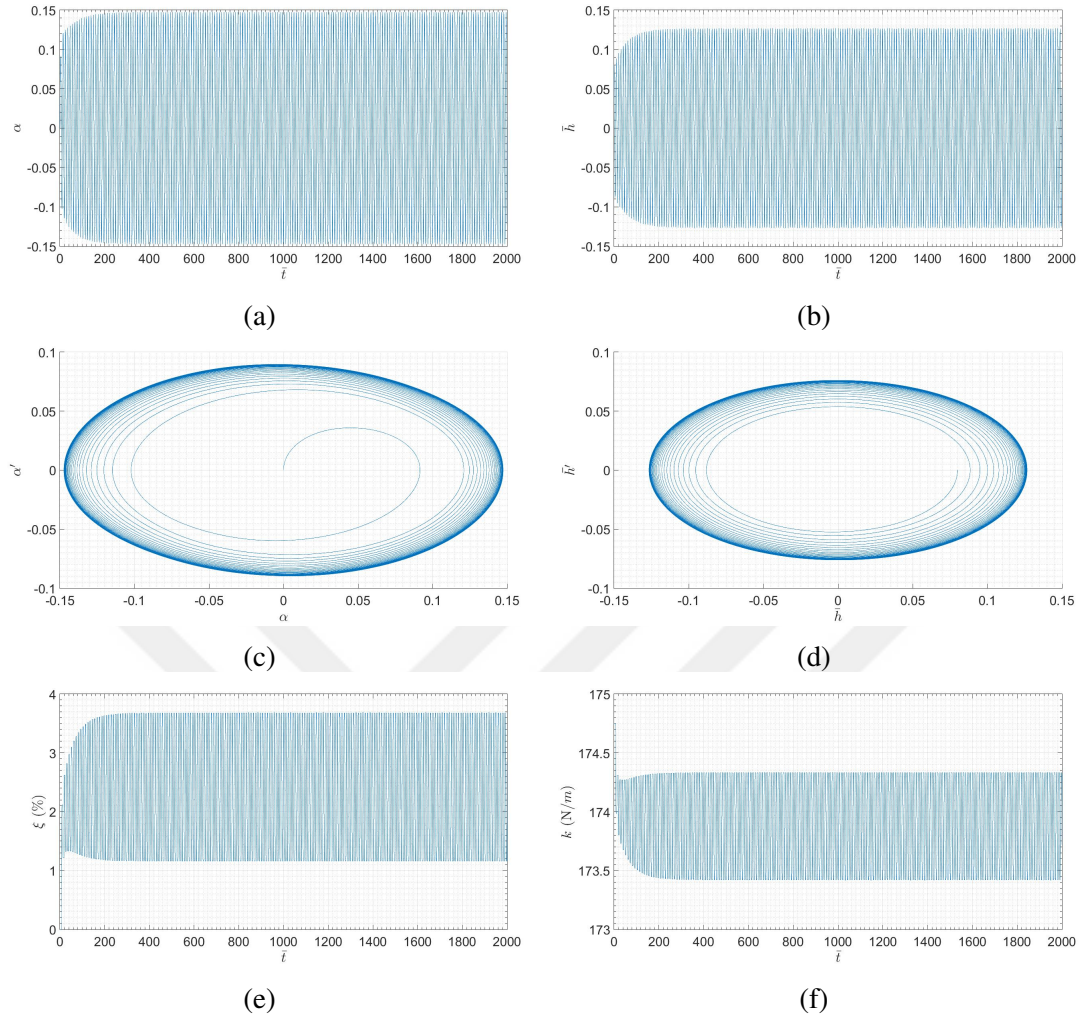

Figure 4.16 : Displacements at 14 m/s for 3.5 N preload (a) pitch displacement with dimensionless time (b) plunge displacement with dimensionless time (c) pitch displacement phase portrait (d) plunge displacement phase portrait and corresponding change in the (e) martensite fraction (f) stiffness.

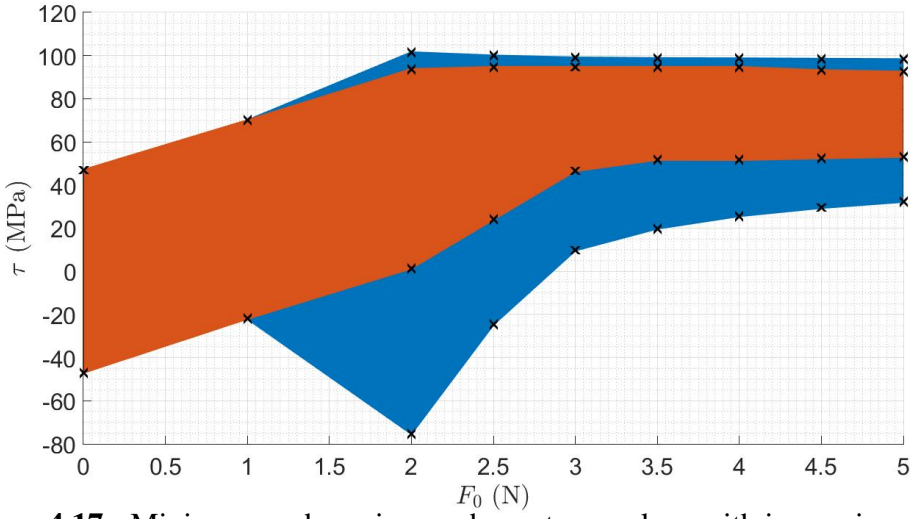

Figure 4.17 : Minimum and maximum shear stress values with increasing preload values for flutter and post-flutter speeds.

5. CONCLUSION

In this thesis, analysis of 2 degrees of freedom aeroelastic airfoil section modeling with shape memory alloy springs which has superelastic effects. The main idea is absorbing unwanted increasing oscillations when an airfoil is subjected to the airflow with using nonlinear damping effects related to phase transformations between austenite phase and martensite phase of shape memory alloy springs. For this reason, the steel spring in the pitch degrees of freedom is replaced by a shape memory alloy spring with the intent of converting growing oscillations to the acceptable limit cycle oscillations under specific constraints on flutter and post-flutter conditions.

The shape memory alloy material specifications that used in this thesis are based on Brinson (1993) and related shape memory alloy helical spring design is derived from Liang and Rogers (1997). The aeroelastic airfoil section with shape memory alloy spring parameters are included in the classical aeroelastic equations of motion. For defining the airflow the unsteady aerodynamic model of Edwards (1977) that is a state-space representation of Jones (1938) approximation to Wagner indicial function for arbitrary airfoil motion is used. This complex equations of motions are solved numerically with the fourth order Runge-Kutta method.

In chapter 2, the detailed shape memory alloy material specifications, phase transformations, damping capabilities and applications and shape memory alloy spring design are represented. In chapter 3, the detailed aeroelastic system, deriving equations of motions and the including of shape memory alloy spring to the aeroelastic system are discussed. Also, equations of motion for the aeroelastic system derived and converted to dimensionless state-space representation for good compatibility with the state-space representation unsteady aerodynamic model of Edwards. In chapter 4, first the classical aeroelastic airfoil section analysis and structural behavior of shape memory alloy springs are mentioned. Then, the aeroelastic system behavior with shape memory alloy spring (in pitch degrees of freedom) and some preload values is investigated at linear flutter and post-flutter speeds. It is observed that the aeroelastic system with the shape

memory alloy spring shows same behaviors like with steel spring for a specific limit of preload values (2 N). After reaching criticial stress value with this preload value, the amplitudes of oscillations are absorbed and decreased by shape memory alloy spring's nonlinear superelastic effects with increasing preload values. When the preloads were applied, it was observed that the obtained oscillation amplitudes decreased by 50% compared to the obtained oscillation amplitudes without the preload. In the post-flutter case, the destructive oscillations can be converted by acceptable limit cycle oscillations owing to the damping capabilites and dissipative properties of shape memory alloy springs. Also, the results are shown with graphical and comparative plots in the figures.

REFERENCES

[1] **Gandhi, F. and Chapuis, G.** (2002). Passive damping augmentation of a vibrating beam using pseudoelastic shape memory alloy wires, *Journal of Sound and Vibration*, *250*(3), 519–539.

[2] **Machado, L. and Lagoudas, D.** (2006). Nonlinear dynamics of a SMA passive vibration damping device, *Smart Structures and Materials*, *6169*, 240–251.

[3] **Fosdick, R. and Ketema, Y.** (1998). Shape memory alloys for passive vibration damping, *Journal of Intelligent Material Systems and Structures*, *9*(10), 854–870.

[4] **Casciati, F. and Faravelli, L.** (2009). A passive control device with SMA components: from the prototype to the model, *The Journal of International Association for Structural Control and Monitoring*, *16*(7-8), 751–765.

[5] **Biffi, C.** (2012). Numerical and experimental characterizations of damping properties of SMAs composite for vibration control systems, *Journal of Materials Engineering and Performance*, *21*, 2713–2718.

[6] **Aguiar, R.A.A., S.M. and Pacheco, P.** (2010). Experimental and numerical investigations of shape memory alloy helical springs, *Smart Materials and Structures*, *19*(2), 025008.

[7] **Tanaka, K., K.S. and Sato, Y.** (1986). Thermomechanics of transformation pseudoelasticity and shape memory effect in alloys, *International Journal of Plasticity*, *2*(1), 59–72.

[8] **Liang, C. and Rogers, C.** (1990). One-dimensional thermomechanical constitutive relations for shape memory materials, *Journal of Intelligent Material Systems and Structures*, *1*(2), 207–234.

[9] **Liang, C. and Rogers, C.** (1992). A multi-dimensional constitutive model for shape memory alloys, *Journal of Engineering Mathematics*, *26*, 429–443.

[10] **Brinson, L.** (1993). One-dimensional constitutive behavior of shape memory alloys: thermomechanical derivation with non-constant material functions and redefined martensite internal variable, *Journal of Intelligent Material Systems and Structures*, *4*(2), 229–242.

[11] **Liang, C. and Rogers, C.** (1997). Design of shape memory alloy springs with applications in vibration control, *Journal of Intelligent Material Systems and Structures*, *8*(4), 314–322.

[12] **Hodges, D. and Pierce, G.**, (2011). *Introduction to Structural Dynamics and Aeroelasticity*, Cambridge University Press, Cambridge, 2 edition.

[13] **Dowell, E.**, (2015). *A Modern Course in Aeroelasticity*, Springer, Durham, 5 edition.

[14] **Ostachowicz, W., K.M. and Zak, A.** (2000). Dynamics and buckling of a multilayer composite plate with embedded SMA wires, *Composite Structures*, *48*, 163–167.

[15] **Barzegari, M.** (2012). Aeroelastic characteristics of cantilever wing with embedded shape memory alloys, *Acta Astronautica*, *79*, 189–202.

[16] **Donadon, M. and Faria, A.** (2016). Aeroelastic behavior of composite laminated shells with embedded SMA wires under supersonic flow, *Aerospace Science and Technology*, *52*, 157–166.

[17] **Malher, A., D.O. and Touze, C.** (2017). Influence of a hysteretic damper on the flutter instability, *Journal of Fluids and Structures*, *68*, 356–369.

[18] **Sousa, W. and De Marqui Jr, C.** (2014). Effect of pseudoelastic hysteresis of shape memory alloy springs on the aeroelastic behavior of a typical airfoil section, *Journal of Intelligent Material Systems and Structures*, *27*(1), 1–17.

[19] **Otsuka, K. and Wayman, C.**, (1998). *Shape Memory Materials*, Cambridge University Press, Cambridge.

[20] **Lecce, L. and Concilio, A.**, (2015). *Shape Memory Alloy Engineering for Aerospace, Structural and Biomedical Applications*, Butterworth-Heinemann Publications, Oxford.

[21] **Lagoudas, D.**, (2008). *Shape Memory Alloys*, Springer, New York.

[22] **Wayman, C.** (1992). Shape memory and related phenomena, *Progress in Materials Science*, *36*, 203–224.

[23] **Sousa, V.C.** (2016). Effects of superelastic shape memory springs on the aeroelastic behavior of a typical airfoil section: passive vibration attenuation and energy harvesting applications, *Ph.D. thesis*, UNESP, Sao Paulo, BRAZIL.

[24] **Edwards, J.W., A.H. and Breakwell, J.** (1979). Unsteady aerodynamic modeling for arbitrary motions, *AIAA Journal*, *17*(4), 365–374.

[25] **Theodorsen, T.**, (1935), General theory of aerodynamic instability and the mechanism of flutter (Report No. 496). Washington : National Advisory Committee for Aeronautics.

[26] **Jones, R.**, (1939), The unsteady lift of a finite wing (Report No. 682). Washington : National Advisory Committee for Aeronautics.

CURRICULUM VITAE

Name Surname : Osman DAĞLI

Place and Date of Birth : İstanbul - 08.10.1991

E-Mail : odagli@hho.edu.tr

EDUCATION:

- **B.Sc.** : 2016, Abant İzzet Baysal University, Faculty of Engineering, Mechanical Engineering

PROFESSIONAL EXPERIENCE AND REWARDS:

- 2016 Abant İzzet Baysal University Mechanical Engineering Department highest ranked student.
- 2015-2016 Mechanical Engineer at Polidoor Industrial Door Systems
- 2016-2019 CAD/CAM/Manufacturing Engineer at Metal Yapı Holding
- 2019- CAD/CAM/Manufacturing Engineer at Metal Yapı Holding

PUBLICATIONS, PRESENTATIONS AND PATENTS ON THE THESIS:

- **Dağlı O., Kaya M. O., Öner U.** 2020:, Şekil Hafızalı Alaşım Yayı ile Modellenmiş Kanat Profilinin Aeroelastik Analizi. VIII. Ulusal Havacılık ve Uzay Konferansı, THKÜ, September 9-11 2020, Ankara, Turkey.